Identification of a New Zinc Binding Chemotype by Fragment Screening

Identification of a New Zinc Binding Chemotype by Fragment Screening

Panagiotis K. Chrysanthopoulos[1,#], Prashant Mujumdar[1,#], Lucy A. Woods[1], Olan Dolezal[2], Bin Ren[2], Thomas S. Peat[2,*] and Sally-Ann Poulsen[1,*]

[1]Griffith University, Griffith Institute for Drug Discovery, Nathan, Brisbane, Queensland 4111, Australia

[2]CSIRO, Biomedical Manufacturing Program, 343 Royal Parade, Parkville, Melbourne, Victoria 3052, Australia

[#]Equal first authors

Email s.poulsen@griffith.edu.au, tom.peat@csiro.au

Abstract

In this manuscript we report the discovery of a new zinc binding chemotype from screening a non-biased fragment library. Using the orthogonal fragment screening methods of native state mass spectrometry and surface plasmon resonance, two 3-unsubstituted-2,4-oxazolidinedione fragments, compounds **10** and **11**, were found to have low micromolar binding affinity to the zinc metalloenzyme carbonic anhydrase II (CA II). This affinity approached that of fragment sized primary benzene sulfonamides, the classical zinc binding group found in most CA II inhibitors. Protein X-ray crystallography established that the 3-unsubstituted-2,4-oxazolidinedione fragment bound to CA II via an interaction of the acidic ring nitrogen with the CA II active site zinc, as well as a hydrogen bond between the oxazolidinedione ring oxygen and the CA II protein backbone. We then synthesised a panel of fragment analogues by interchanging O, N and S heteroatoms to establish structure-activity relationship (SAR) for the zinc binding capacity of oxazolidinedione, thiazolidinedione, hydantoin, thiohydantoin and rhodanine chemotypes for CA affinity, these chemotypes have not been tested for binding to CAs previously. We propose that 3-unsubstituted-2,4-oxazolidinediones are a viable starting point for the development of an alternative class of CA inhibitor to rival the classic primary sulfonamide class, wherein the medicinal chemistry pedigree has already spanned several decades.

Introduction

Proteins that require a metal cofactor for function have gained significant traction as therapeutic targets,[1, 2] with the mechanism of action of a number of clinically approved drugs and investigational compounds attributed to metalloenzyme inhibition.[3-6] Zinc is one of the most abundant metal cofactors in the human proteome[7, 8] and small molecule zinc metalloenzyme inhibitors usually comprise a zinc binding pharmacophore[9] that interacts directly with the metal ion to block endogenous activity.[10-12] The importance of zinc proteins is exemplified in recent studies that show a correlation between zinc recruitment and the complexity of eukaryotic genomes.[13] There are a number of zinc binding groups (ZBGs) that have been explored in exquisite structural detail for binding to zinc metalloenzymes, these include the carboxylate, hydroxymate, sulfonamide, thiol and phosphonate functional groups. These functional groups are well represented in the ligands of zinc metalloprotein-ligand structures that have been deposited with the protein data bank (PDB) and in approved drugs targeting metalloenzymes.[14] With the advent of fragment based drug discovery (FBDD) has come a new opportunity to discover alternate and novel metal binding groups by fragment screening.[15] Fragment screening represents a dramatic change in the approach to drug discovery that makes use of low molecular weight small molecules (i.e. fragments) for unbiased identification of novel structural motifs that bind to proteins with high ligand efficiency. A hit fragment may be structurally elaborated to a new chemical entity with drug-like properties and functionality to improve strength and specificity of binding interactions with the target protein. Since 2005, fragment screening has resulted in more than 30 drug candidates that have entered clinical trials, with two U.S. Food and Drug Administration (FDA) approved drugs and several more compounds in advanced trials.[16] The relatively short timeframe from fragment to U.S. FDA approved drugs has led to take-up of fragment screening approaches in academia, biotech and pharma.[16] A combination of FBDD with metalloprotein targets has been the focus of several successful FBDD campaigns

by Cohen and colleagues utilising fragment libraries assembled from pharmacophores that have a known predilection toward metal binding.[12, 17, 18] Additionally, Klebe and colleagues have characterised the structure of a number of alternate ZBGs for carbonic anhydrase II (CA II, EC 4.2.1.1).[19]

Our group is interested in modulating carbonic anhydrase (CA) activity for therapeutic purposes and has previously targeted inhibition of this zinc metalloenzyme using both standard and novel medicinal chemistry strategies.[20-24] hCAs (h = human) regulate pH homeostasis by catalysing the reversible hydration of carbon dioxide to bicarbonate and a proton: $CO_2 + H_2O \leftrightarrows HCO_3^- + H^+$ and evidence is mounting that modulating tumour cell pH homeostasis may prove an effective anti-tumour strategy.[24-26] The CA active site zinc coordinates to the imidazole sidechain of three histidine residues and to the H_2O molecule involved in the CO_2 hydration reaction, hence the implied target of small molecule CA inhibitors is the CA active site zinc. A key focus of our novel CA targeting strategies has been the discovery of new chemical entities as these are critical for the drug discovery pipeline to deliver new CA-based therapeutics.[27] We recently reported two novel sulfonamide compounds, the natural product Psammaplin C (**1**)[28] and the saccharin glycoconjugate (**2**),[22] as potent, isozyme selective inhibitors of CAs, Figure 1A.

More recently we reported the findings of an unbiased fragment screening campaign targeting CA II.[29] Seven fragment hits (**3-9**) were identified, including the known ZBGs of primary sulfonamide (fragment **3**) and carboxylate (fragments **4-6**), Figure 1B.[29-33] More interesting however was the finding of two 5-substituted tetrazoles (fragments **7** and **8**) and a 3-substituted-1,2,4-triazole (fragment **9**) as hits, Figure 1B. Fragments **7-9** are not classic acidic functional groups like carboxylates and sulfonamides, but instead may be considered as acidic

heterocycles. Additionally these heterocycles were not previously known as CA II binding chemotypes, ZBGs or metal binding groups generally. The primary sulfonamide fragment **3** displayed strongest CA II binding (K_D = 1.4 μM) while fragments **4-9** were much weaker binders (K_D range 631 - 1280 μM).[29] The strong binding affinity of the primary sulfonamide functional group for CA II compared to other known ZBGs is attributed to two key hydrogen bonds with the active site threonine residue, that are in addition to the zinc-sulfonamide interaction, Figure 2. This binding pose has been observed for >200 sulfonamide:CA II complexes reported in the PDB. The specificity of the two key hydrogen bonds ensures that the sulfonamide ZBG has very high selectivity for CA with minimal binding to other zinc metalloenzymes.[34] Using X-ray crystallography we showed that the carboxylate and tetrazole moieties of fragments **4-8** interact with the active site zinc of CA II (either directly or via an intervening water molecule), some also formed interactions to the active site residues Thr199, Thr200 (both backbone and side chains). We were unable to obtain a crystal structure of CA II bound to triazole fragment **9**.

In this manuscript we report the discovery of a new zinc binding chemotype that was detected by fragment screening of an unbiased fragment library against CA II. We show that the 3-unsubstituted-2,4-oxazolidinedione fragment, not previously known for zinc binding, exhibits particularly strong binding affinity for CA II that approaches that of the primary sulfonamide ZBG of classical CA inhibitors. We have defined the structural basis for the strong binding and have detailed structure-activity relationship (SAR) boundaries for the oxazolidinedione and related chemotypes for CA affinity using a combination of chemical design and synthesis to prepare fragment analogues followed by biophysical characterisation of new fragment analogues with native state mass spectrometry (MS), surface plasmon resonance (SPR) and protein X-ray crystallography (XRC). We have utilised MS for qualitative, semi-quantitative

and quantitative fragment screening and to evaluate fragment SAR, known as "SAR by MS".[35] The discovery of the 3-unsubstituted-2,4-oxazolidinedione fragment as a new ZBG contributes to the growing importance of small molecule CA inhibitors that comprise non-classical features, as well as alternate and novel ZBGs for drug development generally.

A.

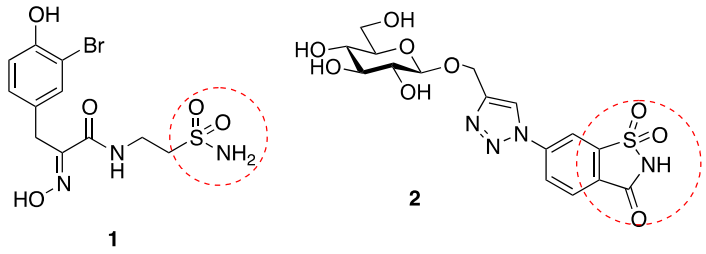

B.

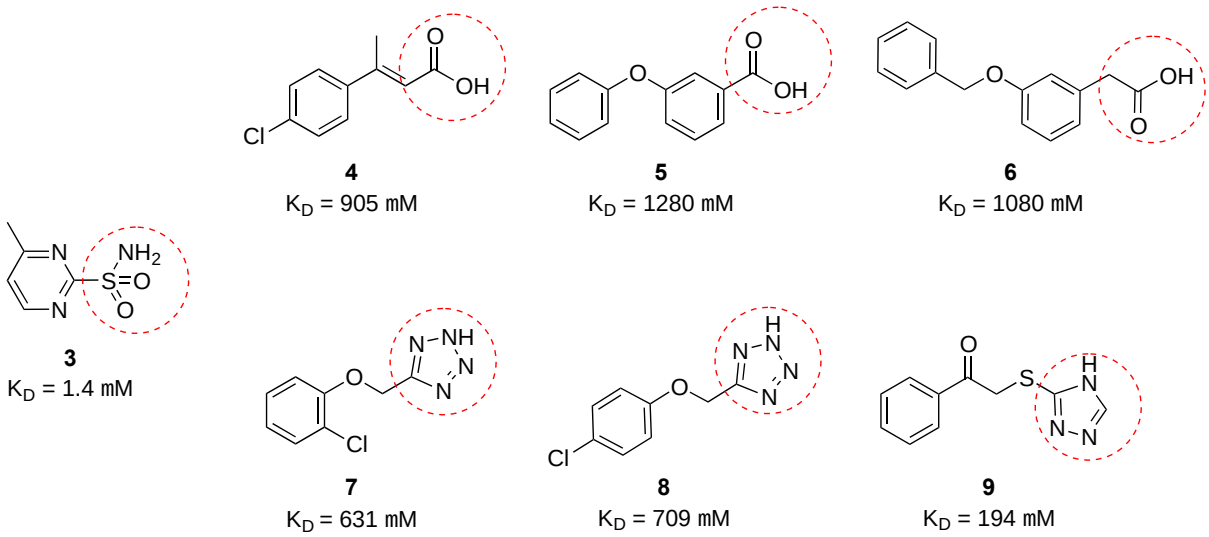

Figure 1. A) Unusual carbonic anhydrase (CA) inhibitors Psammaplin C (**1**)[28] and saccharin glycoconjugate (**2**)[22]. B) Fragment hits (**3-9**) identified from an unbiased fragment screening campaign targeting CA II.[29] The known or probable zinc binding group of each fragment is circled.

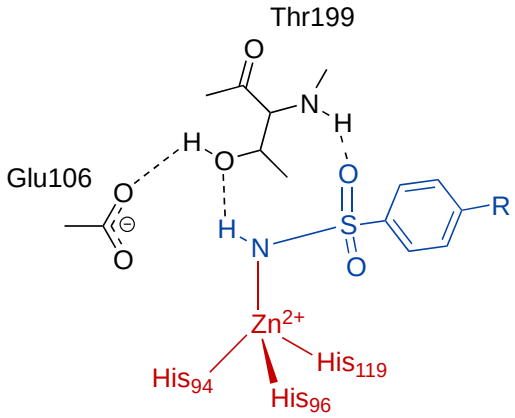

Figure 2. Common binding pose observed for >200 primary sulfonamide:CA II complexes reported in the Protein Data Bank.[36]

Results and Discussion

1-Phenyl-2,4-oxazolidinedione **10** and 1-(2′,4′-dimethoxyphenyl)-2,4-oxazolidinedione **11**, were identified and validated as binders for hCA II by fragment screening of a non-biased synthetic fragment library using orthogonal fragment screening techniques: SPR and native state mass spectrometry, Figure 3A. The binding affinities (K_D) of **10** and **11** for hCA II are 3.5 μM and 6.1 μM, respectively, as determined by SPR. These affinities are 2-3 orders of magnitude stronger than that for the non-sulfonamide fragments **4-9** (K_D range 631 - 1280 μM), and similar to that of the sulfonamide fragment **3** (K_D = 1.4 μM), reported by us recently.[29] We were keen to investigate the structural basis of the strong binding of **10** and **11** to hCA II and to establish if the 3-unsubstituted-2,4-oxazolidinedione heterocycle is a viable starting point for the development of a new class of CA inhibitor to rival the classic primary sulfonamide chemotype, wherein the medicinal chemistry pedigree has already spanned several decades. We determined the protein X-ray crystal structure of fragments **10** and **11** bound to hCA II, Figure 3B. The fragments bound via an interaction of the acidic ring nitrogen with the hCA II active site zinc. The pK_a value for the -NH- of **10** (pK_a of 5.5) together with the pK_a values of a series

of phenyl and benzyl substituted five membered heterocycles predicted to be acidic bioisosteres were measured more than 25 years ago to acquire data for the calculated Log P (cLog P) database, Pomona College MedChem CLOGP.[37] The hCA II:**10** and hCA II:**11** structures are consistent with the prediction that 3-unsubstituted-2,4-oxazolidinedione is an acidic bioisostere.[37] In addition to the zinc binding interaction there is a hydrogen bond (2.9-3.0 Å) formed between the ring –O– of **10** and **11** with the Thr199 backbone nitrogen, akin to the primary sulfonamide binding pose, this hydrogen bond likely accounts for the increased binding affinity.

We next searched the PDB against the 3-unsubstituted-2,4-oxazolidinedione fragment and identified only one protein:ligand crystal structure where the ligand comprises this fragment, the ligand is (5*R*)-5-(3-{[3-(5-methoxybenzisoxazol-3-yl)benzimidazol-1-yl] methyl}phenyl)-5-methyloxazolidinedione (**12**, Figure 3A) in complex with the peroxisome proliferator-activated receptor γ subtype (γPPAR).[38] γPPAR is involved in regulating glucose metabolism and insulin sensitivity, and γPPAR modulation has potential for development of treatment of type 2 diabetes mellitus.[38] The oxazolidinedione moiety of **12** was incorporated as a replacement for a phenoxycarboxylic acid group of a lead compound series. The structure of the γPPAR:**12** complex (PDB ID 3TY0) indicates there are hydrogen bond interactions of the oxazolidinedione to the Ser342 backbone nitrogen and the His266 side chain nitrogen of γPPAR. Notably γPPAR is not a metalloprotein hence there is no opportunity for a metal binding interaction in this protein.[38] The finding that **10** and **11** bind to the hCA II active site zinc coupled with the lack of exemplar 3-unsubstituted-2,4-oxazolidinedione fragments as a ZBG in the PDB establishes the 3-unsubstituted-2,4-oxazolidinedione as a new zinc binding chemotype.

A.

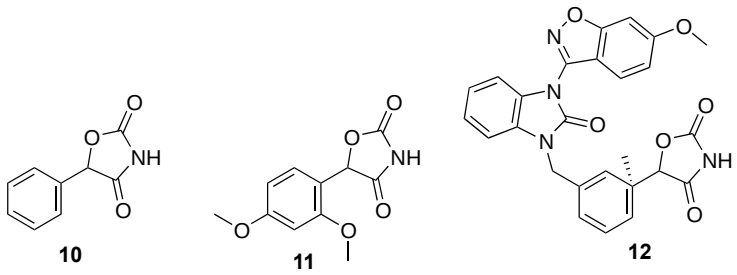

B.

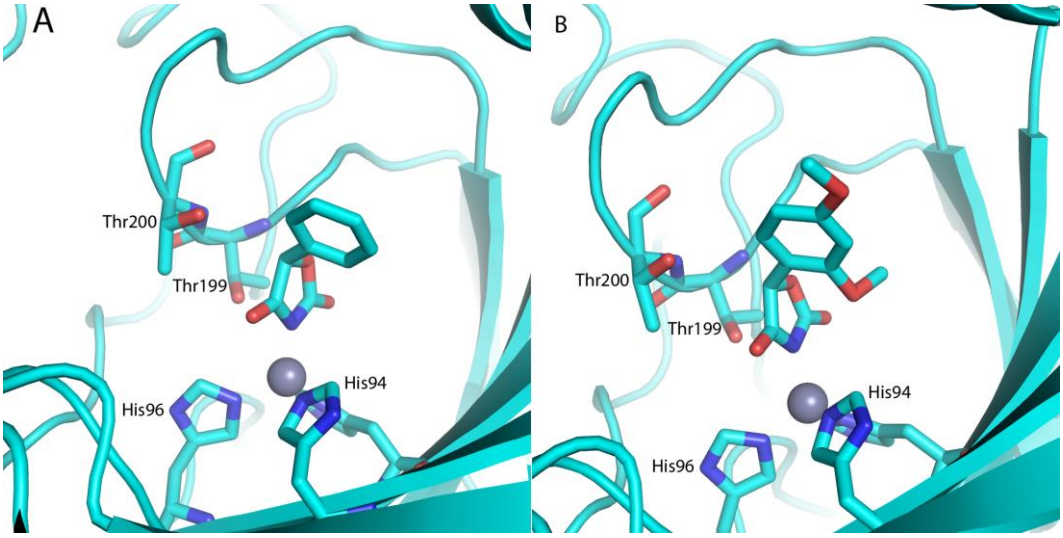

Figure 3. (A) 3-Unsubstituted-2,4-oxazolidinediones **10**, **11** (this study) and γPPAR inhibitor **12**.[38] (B) Crystal structures of **10** and **11** with carbonic anhydrase II (CA II). In panel A, **10** is shown in the crystal structure with the zinc atom represented by a grey sphere and active site residues labelled (His94, His96, Thr199, Thr200; His119 is hidden behind the zinc and His94). In panel B, **11** is shown in approximately the same orientation as **10**, with the same active site residues labelled as in panel A.

Compound design to establish SAR

To ascertain the structure-activity relationships (SAR) for binding of the oxazolidinedione fragment to CAs, a series of structural modifications were made to the heteroatoms and to the 5-substituent with the acidic cyclic imide NH group retained in all compounds. The SAR fragment library comprised lead fragments **10** and **11** (Figure 3) and new fragments **13** – **29**, Figure 4. Specifically, the replacement of the ring heteroatom from –O– (oxazolidinediones, **10** and **11**) to either a –S– (thiazolidinediones, **13**, **14**, **16** and **17**) or–NH– (hydantoins, **15**, **18**, **19**, **20** and **21**) was examined to determine the effect of both hydrogen bond acceptor strength (–O– versus –S–) and modification of a hydrogen bond acceptor to a hydrogen bond donor (–O– and –S– versus –NH–), noting the key role of the ring oxygen in the **10**:CA II and **11**:CA II crystal structures as a hydrogen bond acceptor (~3.0 Å to Thr199 N). We also modified both the ring heteroatom from –O– to –NH– (hydrogen bond acceptor to hydrogen bond donor) together with one of the carbonyls to a thiocarbonyl (thiohydantoins, **26** and **27**). Depending on ease of synthesis, these heteroatom changes were combined with modification of the 5-substituent (phenyl, benzyl or benzylidene derivatives) with or without added methoxy electron withdrawing groups. Additionally, the replacement of both the –O– heteroatom and the 4-carbonyl oxygen with sulfur atoms denotes the rhodanine heterocycle (rhodanines, **22**, **23**, **24** and **25**), which has further altered hydrogen bonding capacity compared to **10** and **11**. To the best of our knowledge the thiazolidinedione, hydantoin, thiohydantoin and rhodanine chemotypes have not been tested for binding to or inhibition of CAs and will be useful to establish SAR. Finally, we included two FDA approved fragment-sized oxazolidinediones, the anticonvulsant trimethadione **28** and its demethylated metabolite dimethadione **29**, Figure 4, in the SAR fragment library. The final assembled fragment library to establish SAR thus comprised 19 fragments (**10**, **11**, **13** – **29**) of molecular weight <300 Da.

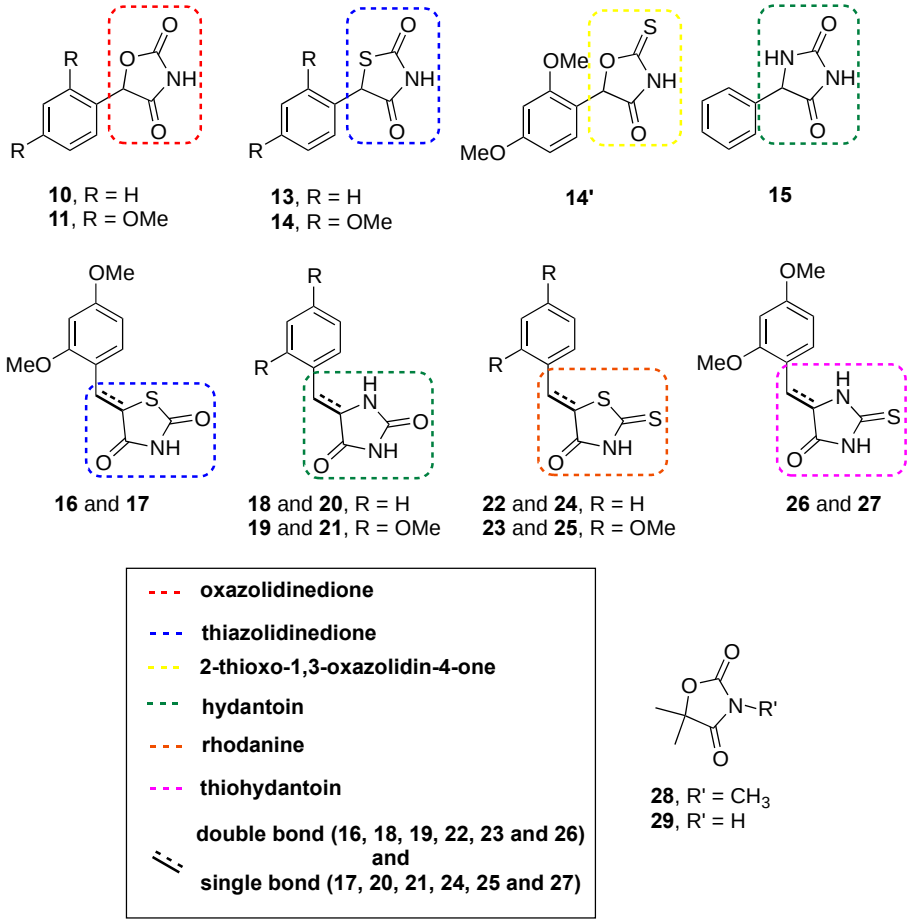

Figure 4. New fragment library members **13**–**29**, selected to establish SAR around the oxazolidinedione ZBG chemotype for CA inhibition. The structure of **14** was revised to **14′** following X-ray crystallography.

Compound Screening

In a recent fragment screening study we reported on the suitability of native state nanoelectrospray ionization mass spectrometry (nanoESI-MS) for fragment screening, highlighting numerous favourable attributes of the method including the ability to readily detect protein−ligand noncovalent complexes where K_Ds were in the mM range.[29] This fragment screening method consumed minimal protein, did not utilise excess fragment concentrations and provided rapid results. There was also very good overlap with hits identified using SPR (as

the primary screen) and X-ray crystallography (to determine fragment hit binding pose).[29] Native state mass spectrometry has been applied to the study of noncovalent protein-ligand interactions for the measurement of K_D values,[39, 40] there are however few examples of mass spectrometry for fragment screening,[29, 41-45] and mass spectrometry is not yet fully evaluated as a primary fragment screening method. In the present study, screening of the new fragment library members **13**–**29** and previously identified hit fragments **10** and **11**, was carried out first using native state mass spectrometry, followed by SPR for validation. Finally X-ray crystallography was employed to provide a detailed analysis of protein-fragment interactions for validated hits.

Nanoelectrospray ionization (nanoESI) mass spectra were acquired with test samples comprising CA II with one equivalent of added fragment (**10**, **11**, **13** – **29**). Nine fragments were observed bound to CA II - **10**, **11**, **13**, **14** (revised to **14′** following X-ray crystallography), **17**, **22**, **24**, **25** and **27 (**revised to a mixture of **27/27′** following X-ray crystallography). The observation of [protein + fragment] complex in the nanoESI mass spectrum enables qualitative classification of a fragment as a hit (or "binder") or non-hit (or "non-binder"), with arbitrary thresholds possible to further delineate fragment binding as strong, medium or weak. To incorporate quantification to the nanoESI method we introduce here the concept of mass spectrometry fragment affinity (FA_{MS}), specifically we assess the potential of the FA_{MS} metric to quickly and accurately quantify the relative binding strength from mass spectrometry data. FA_{MS} is expressed as a percentage and is determined from the fraction of the intensity of the [protein + fragment] peaks relative to total protein peaks, Equation 1, where $I_{[P:F]}$ and $I_{[P]}$ are the mass spectrometric peak intensities of the [protein + fragment] complexes and free/acetate bound protein, respectively, in the ESI mass spectrum. FA_{MS} values for CA II and fragment,

when equimolar amounts of protein and fragment (7.5 μM each) are analysed, are in Table 1 (columns 3 and 4).

$$FA_{MS} = \frac{I_{[P:F]}}{I_{[P:F]}+I_{[P]}} \times 100\% \qquad \text{Equation 1.}$$

Next K_D values were determined for eight of the hit fragments (insufficient sample of **14′** available at time of experiment). Experiments were performed with CA II (14.5 μM) titrated against at least five different fragment concentrations ([F] range 0.5 μM - 120 μM) until either full complexation was observed (i.e. $I_{[P]} = 0$) or the fragment concentration reached 120 μM. The FA_{MS} was calculated for each fragment concentration and values plotted against fragment concentration [F]. The K_D was calculated upon curve fitting this plot based on Hill slope analysis, Figure 5.[46] K_Ds determined by nanoESI-MS ranged from 2.3-50.7 μM, (Table 1, columns 5 and 6). Representative mass spectra showing the +10 charge state acquired for the CA II + **24** titration (K_D = 16.7 μM) are presented in Figure 6. All observed charge states (+9, +10 and +11) were utilised for both FA_{MS} and K_D calculations (Table 1, columns 3 and 5). Additionally for comparison, FA_{MS} and K_D calculations were performed using only the peak intensities for the +10 charge state, (Table 1, columns 4 and 6). The single charge state (+10 only) calculated values are in excellent agreement with calculated values using all charge states (+9, +10 and +11), indicating that the single charge state calculation of FA_{MS} and K_D will be sufficient for future fragment screening campaigns using nanoESI-MS. The method employed for all the nanoESI-MS analyses has been optimised to ensure gentle conditions and avoid in-source dissociation, so that the observed peak ratios in the mass spectra reflect the solution concentrations. The ionisation efficiency of the free protein and the protein:fragment complex is assumed the same. It is also noted that the equimolar FA_{MS} values provide a useful rank order of affinity compared to K_D calculations determined from more laborious and higher sample

consuming titration experiments, the overall trend is consistent, while for the weaker bound fragments in particular (**17**, **22** and **27/27′**) the correlation is excellent.

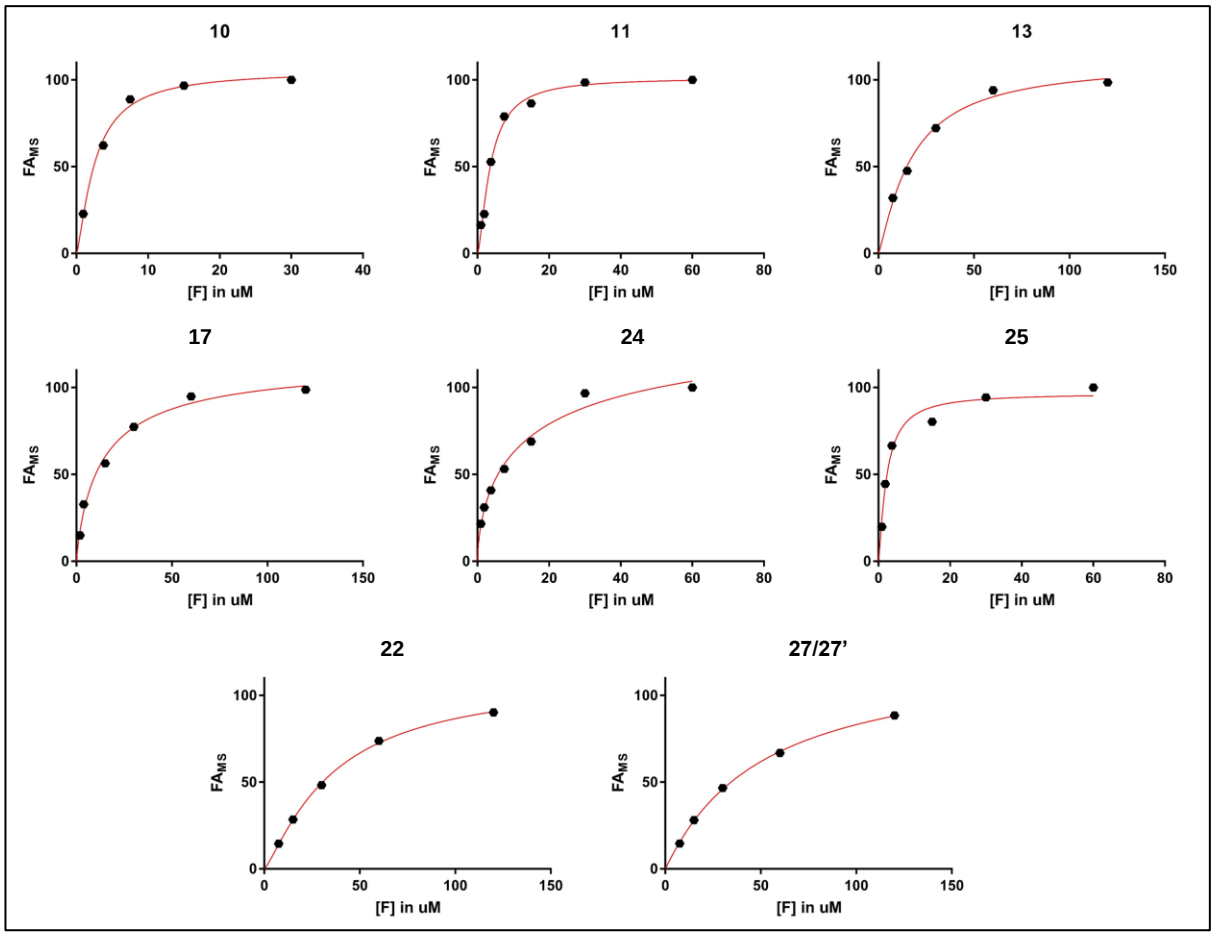

Figure 5. Saturation curves of the nanoESI-MS titration of eight hit fragments with CA II (14.5 μM). FA_{MS}, as calculated at each fragment concentration using all observed charge states (+9, +10 and +11), is plotted against total fragment concentration [F] with curve fitting based on Hill slope analysis used to determine K_D.[46]

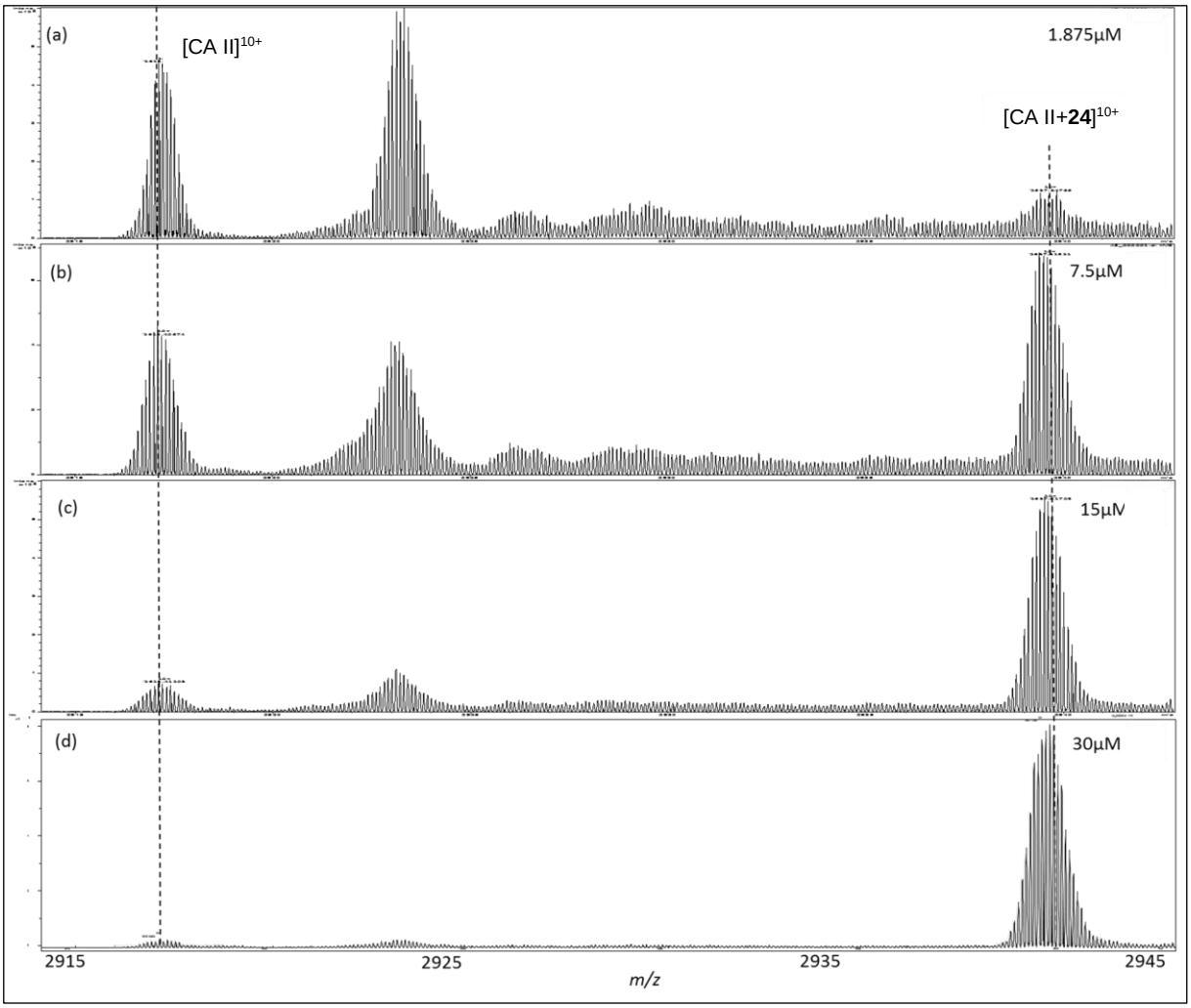

Figure 6. Representative positive ion mode nanoESI mass spectra (+10 charge state) of 14.4 µM hCA II (pH 7.4 10 mM NH_4OAc) titrated with fragment **24** to determine fragment K_D by nanoESI-MS: (a) 1.875 µM of **24**; (b) 7.5 µM of **24**; (c) 15 µM of **24**; and (d) 30 µM of **24**.

SPR was used as a secondary orthogonal fragment screening method for fragments **10**, **11**, **13**–**29**. Minimally biotinylated CA II was immobilised on a SPR sensor chip surface via biotin-streptavidin interactions, and the SAR fragment library analysed in dose-response experiments, performed at 25 °C across a 5-point fragment concentration series range, to determine the K_D of the fragments, Table 1 (column 2). SPR analysis identified the same nine fragments (**10**, **11**, **13**, **14** (revised to **14′** following X-ray crystallography), **17**, **22**, **24**, **25** and **27** (revised to a mixture of **27**/**27′** following X-ray crystallography)) that bound to CA II as identified by

nanoESI-MS, with K_Ds that ranged from 3.4-65.5 μM (excluding **22**), Table 1 (column 2). The K_D values calculated by the nanoESI-MS experiments are in good agreement (K_D range 2.3-50.7 μM) with the values measured in solution by SPR. The only significant discrepancy appears in the K_D values of fragment **22** (nanoESI-MS K_D = 35.8 μM, SPR K_D = 355 μM) however the K_D for **22** could not be reliably determined by SPR due to solubility issues of this compound in the SPR buffer and this issue is likely responsible for the discrepancy observed. Non-binding fragments **15**, **16**, **18-21**, **26**, **28** and **29** were also fully consistent using the orthogonal methods, these fragments exhibited no detectable binding to CA II by either SPR or nanoESI-MS. Fragment **23** was only the only fragment discrepancy between nanoESI-MS and SPR. It was not detected by nanoESI-MS however was detected by SPR. Notably **23** had the weakest binding of the SPR hits (K_D = 1000 μM), much weaker than all other hit fragments. The rank order of K_Ds by the two methods also followed a similar trend: nanoESI-MS K_D values, low to high: **25**, **10**, **11**, **17**, **24**, **13**, **22**, **27/27′**; SPR K_D values, low to high: **25**, **10**, **11**, **24**, **17**, **14′**, **13**, **27/27′**, **22**, **23**. Binding sensorgrams for fragments interacting with the immobilised CA II are provided in Supporting Information. The findings that nanoESI-MS and SPR provide agreement of both the magnitude and trend of K_D values suggests that the straightforward metric FA_{MS}, with equimolar protein and fragment concentrations, offers the opportunity for rapid, semi-quantitative assessment of fragment binding strengths. If nanoESI-MS is selected as a primary screen we propose that MS has potential to accelerate and inform the initial steps of FBDD.

Table 1. Screening results for **10**–**29** using native state mass spectrometry, SPR and protein X-ray crystallography.

Compound No.	**SPR K_D (μM)**	**ESI-MS FA_{MS} (%)**[c]	**ESI-MS FA_{MS} (%)**[d]	**ESI-MS K_D (μM)**[c]	**ESI-MS K_D (μM)**[d]	**Protein XRC**[e]
10	3.5	87.7	79.8	2.6	3.0	Y
11	6.1	88.1	90.2	3.6	3.5	Y
13	32.9	91.5	93.7	17.4	18.4	Y
14′[a]	28.6	51.1	53.1	n.d.[f]	n.d.	Y
15	NSB[b]	NSB	NSB	n.d.	n.d.	n.d.
16	NSB	NSB	NSB	n.d.	n.d.	n.d.
17	26.2	63.9	67.3	13.9	16.0	Y
18	NSB	NSB	NSB	n.d.	n.d.	n.d.
19	NSB	NSB	NSB	n.d.	n.d.	n.d.
20	NSB	NSB	NSB	n.d.	n.d.	n.d.
21	NSB	NSB	NSB	n.d.	n.d.	n.d.
22	355[g]	46.3	41.5	35.8	36.2	N
23	1000	NSB	NSB	n.d.	n.d.	N
24	7.7	84.4	85.5	16.7	19.0	Y
25	3.4	68.7	74.5	2.3	2.7	Y
26	NSB	NSB	NSB	n.d.	n.d.	n.d.
27′[h]	65.5	14.6	23.1	50.7	43.6	Y[h]
28	NSB	NSB	NSB	n.d.	n.d.	n.d.
29	NSB[a]	NSB	NSB	n.d.	n.d.	n.d.

[a]The structure of **14** was revised to **14′** following X-ray crystallography. [b]NSB = No significant binding (K_D>2000 μM); [c]using all observed charge states (+9, +10 and +11); [d]using only +10 charge state; [e]XRC – X-ray crystallography. [f]n.d. – not determined; [g]K_D (SPR) could not be reliably determined due to solubility issues of this compound in the SPR buffer. [h]the electron density of the fragment observed did not correlate with the structure of **27** but instead to an impurity in the sample, later identified as **27′**.

Protein X-ray Crystallography

The hit fragments identified from the orthogonal fragment screening (**10**, **11**, **13**, **14**, **17**, **22**, **23**, **24**, **25** and **27**) were subjected to X-ray crystallography following soaking with CA II crystals as described earlier.[29] Eight of the ten soaked fragments led to CA II:fragment structures observed by X-ray crystallography, all fragments bound via interaction of the acidic imide nitrogen with the hCA II active site zinc (1.9-2.0 Å) and with the Thr199 side chain hydroxyl (3.1-3.2 Å) (Figure 7, Table 2 and Supporting Information). The eight observed fragments include the original oxazolidinedione chemotypes **10** and **11**, the thiazolidinedione chemotypes **13** and **17**, and rhodanine chemotypes **24** and **25**. The structure of thiazolidinedione **14** was revised to 2-thioxo-1,3-oxazolidin-4-one **14′** following X-ray crystallography. The electron density of this fragment clearly showed an exocyclic sulfur (as thiocarbonyl), rather than sulfur within the ring, Figure 7D. Both **14** and **14′** are conceivable products from the synthesis, however they have an identical chemical formula and are also difficult to distinguish using NMR spectroscopy. The thiohydantoin chemotype **27** provided a structure following soaking, however the electron density showed that there was an additional atom attached to C-5 of the ring (Figures 7 and 8) and could not be correlated with the proposed structure of **27**. The electron density observed for **27′** is consistent with either an OH or NH_2 substituent at C-5, Figure 8. We re-examined a sample of **27** by LCMS and HRMS and this showed that the sample was a mixture of **27** (~95%) and the hydrated compound **27′** (~5%) (Figure 8). Co-formation of C-5 benzylidine thiohydantoins with hydrated C-5 hydroxy/C-5 benzyl thiohydantoins has

been reported.[47] As **27′** makes additional interactions over **27**, it is plausible to imagine **27′** easily outcompeting **27** for the CA II binding site. Structures for **10** and **11**, Figure 7A and 7B, were described earlier in the introduction. For thiazolidinediones **13** and **17** (5-10-fold weaker binders than oxazolidinediones **10** and **11**), unlike the hydrogen bond formed with the ring –O– of oxazolidinediones **10** and **11** and the Thr199 backbone nitrogen, there is no corresponding hydrogen bond formed between the ring –S– of **13** and **17** and the Thr199 backbone nitrogen, Figure 7C and 7E. For **14′**, Figure 7D, the thiocarbonyl is too far away from Thr199 to make any reasonable hydrogen bonds, however the ring –O– is 3.1 Å from the backbone nitrogen of Thr199, similar to the distance seen in compounds **10** and **11** (~3.0 Å). Rhodanine **25** (nanoESI-MS K_D = 2.7 μM, SPR K_D = 3.4 μM) and rhodanine **24** (nanoESI-MS K_D = 19 μM, SPR K_D = 7.7 μM) are relatively strong binders, but neither the ring –S– nor the thiocarbonyl of **24** or **25** make any H-bond interactions with CA II, Figure 7F and 7G.

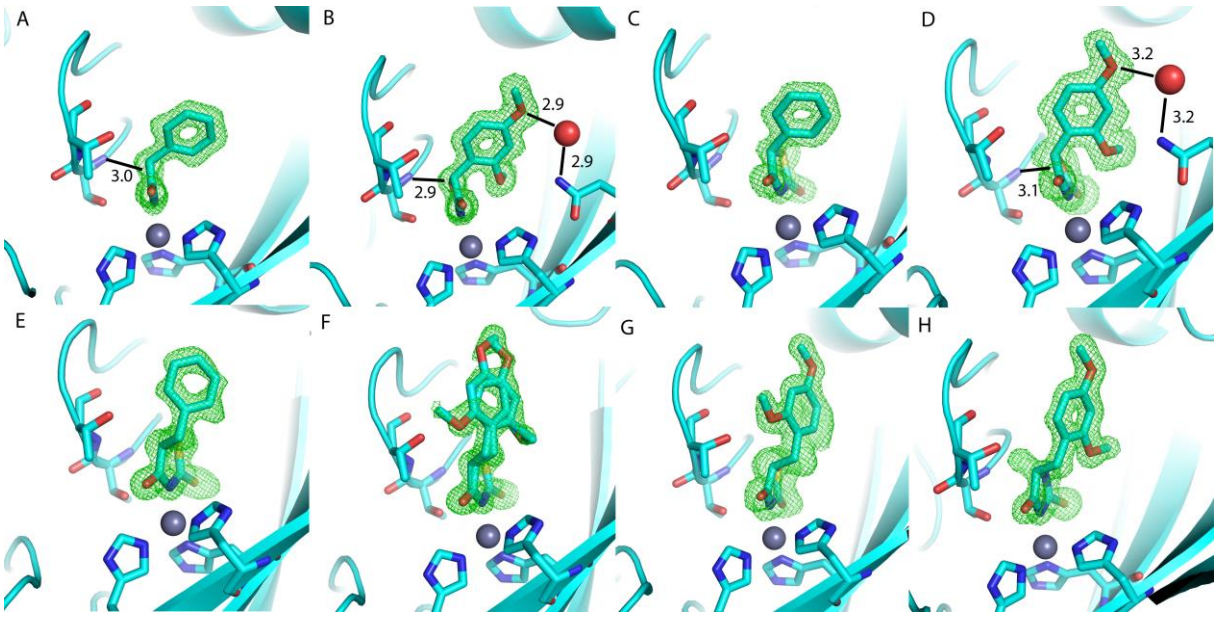

Figure 7. Difference density maps of fragments in the CA II binding site. (A) **10**, oxazolidinedione chemotype. (B) **11**, oxazolidinedione chemotype. (C) **13**, thiazolidinedione

chemotype. (D) **14′** 2-thioxo-1,3-oxazolidin-4-one chemotype. (E) **17**, thiazolidinedione chemotype. (F) **24**, rhodanine chemotype. (G) **25**, rhodanine chemotype. (H) **27**, thiohydantoin chemotype. Difference density (mFo-DFc) for all maps is shown at a 3σ contour level where the fragments were omitted from the model. The active site zinc atom is represented as a grey sphere. Thr199, Thr200 and the three catalytic His residues (His94, His96 and His119) are shown. There is a water molecule (red sphere) within hydrogen bonding distance of a methoxy substituent for compounds **11** and **14′** (B and D). Additionally, for compounds **10**, **11** and **14′** the ring oxygen is within hydrogen bonding distance of the backbone nitrogen of Thr199 and this distance is shown (A, B and D). Also note **24** (F) is modelled in two orientations for the dimethoxyphenyl group whereas the other compounds with this group had one preferred orientation (**11**, **14′**, **25** and **27′**).

Table 2. Interactions of compounds with CA II identified by protein X-ray crystallography.

Compound	**PDB ID**	**Protein-fragment interaction (Å)**				
		Zn-NH	T199OH-NH	T199N-O1	T200NH-OH	T200OH-OH
10	5TXY and 5TY8	1.9	3.2	3.0	-	-
11	5TY9	2.0	3.1	2.9	-	-
13	5TYA	2.0	3.1	-	-	-
14′	5U0D	1.9	3.3	3.1	-	-
17	5U0G	2.0	3.1	-	-	-
24	5U0E	2.0	3.2	-	-	-
25	5U0F	2.0	3.2	-	-	-

27′	5VGY	1.9	3.1	-	2.9	2.6

A.

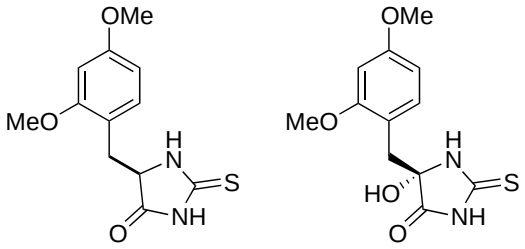

B.

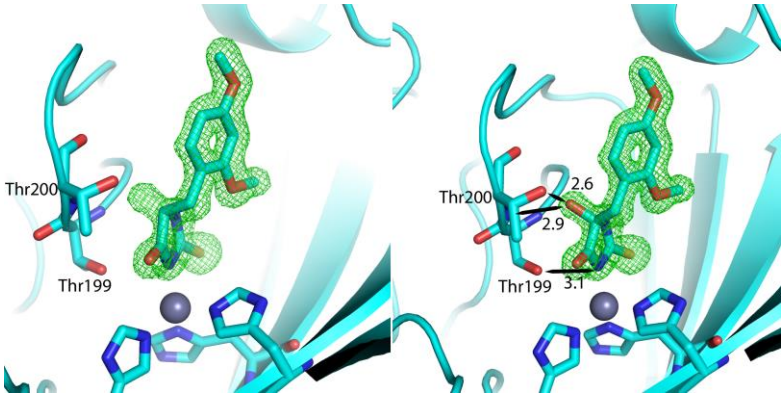

Figure 8. The electron density observed for compound **27** with CA II is consistent with an OH substituent at C-5 (**27′**). Compound **27′** was subsequently identified as a ~5% impurity in **27**. This oxygen makes two potential hydrogen bonds with the Thr200 residue: one at 2.6 Å to the sidechain hydroxyl and another at 2.9 Å to the backbone nitrogen (shown in figure).

The two fragments that failed to provide electron density in the CA II protein X-ray crystal structures were fragments **22** and **23**. As discussed above, fragment **23** was the weakest binding of the ten SPR hits (K_D = 1000 μM) and was not detected by nanoESI-MS. Notably, fragment **22** provided the only significant discrepancy in the K_D values determined by nanoESI-MS and

SPR, however this fragment had solubility issues at the higher concentration required for SPR analysis and this may have affected its ability to be seen in the crystallographic studies as well.

Structure-Activity Relationships

The strong binding properties of oxazolidinediones **10** and **11** shown previously were confirmed in the present study (SPR K_D = 3.5 μM, nanoESI-MS K_D = 2.6 μM and SPR K_D = 6.1 μM, MS K_D = 3.6 μM, respectively). Fragments **10** and **11** have similar affinity, indicating that the two methoxy groups of the dimethoxyphenyl moiety of **11** do not significantly impact on binding even though they introduce steric bulk on to the phenyl ring (*cf.* **10**) and are electron withdrawing. Replacement of the ring –O– of oxazolidinediones **10** and **11** with –S– gave the corresponding thiazolidinedione **13**, this change resulted in a ~10-fold reduction in CA II affinity. The larger size of sulfur relative to oxygen alters the orientation of the ring in the active site, the ring –S– is positioned 3.7 Å from the backbone nitrogen of Thr199, whereas in compounds **10** and **11** the corresponding distance from the ring –O– is 2.9 to 3.0 Å, Table 2. Replacement of the exocyclic carbonyl of oxazolidinedione **11** with a thiocarbonyl gave the 2-thioxo-1,3-oxazolidin-4-one **14′**, this change resulted in a ~10-fold reduction on CA II affinity; however the ring oxygen of **14′** is 3.1 Å from the backbone nitrogen of Thr199, similar to the corresponding interaction of compounds **10** and **11**. The sulfur atom of the thiocarbonyl of **14′** is too far away from Thr199 to make any reasonable hydrogen bonds. The dimethoxybenzyl group of thiazolidinedione **17** was tolerated with one of the methoxy groups making a potential hydrogen bond with the sidechain hydroxyl of Thr200 (3.0 Å), however the more rigid dimethoxybenzylidine group in thiazolidinedione **16** resulted in loss of binding to CA II. Similarly the dimethoxybenzylidine thiohydantoin **26** was a nonbinder, while dimethoxybenzyl thiohydantoin **27′** (an impurity in **27**) was observed (Figure 8) but as a weaker binder (SPR of mixture K_D = 65.5 μM, nanoESI-MS of mixture K_D = 43.6 μM) than **10** and **11**. The introduction

of the –NH– in the ring of hydantoins (**15**, **18 - 21**) abolished binding completely, irrespective of most of the 5-substituents, the exception being **27′** with the added hydroxyl. This SAR suggests that a hydrogen bond acceptor in the ring 1-position (–O–) provides the additional binding affinity observed, this is consistent with the crystal structures for **10** and **11**. Rhodanines **24** (benzyl) and **25** (dimethoxybenzyl) were strong binders, although the electron density shows that the –S– in the ring is too far away from Thr199 to make a hydrogen bond (3.7 Å) compared to the –O– in the ring of lead oxazolidinediones, **10** and **11**. Rhodanines **22** (5-benzylidine substituent) and **23** (5-dimethoxybenzylidine substituent) failed to give a crystal structure while the reduced binding observed by nanoESI-MS and SPR, suggests that the flexibility of the 5-substituent may be important as connection through the sp^2 hybridised carbon of the benzylidine substituents hinders hCA II binding. Rhodanine is identified as a 'PAIN' as this chemotype leads to pan-assay interference.[48] Our findings indicate that CA II is a possible off-target enzyme of 5-subtituted rhodanine compounds, but that any binding is likely dependent also on the nature of the 5-substituent. To the best of our knowledge, CA II as an off-target of rhodanines was not previously known, given that CA II is a ubiquitous enzyme this finding may provide further caution on the decision to advance rhodanine compounds in medicinal chemistry campaigns. Benzylidine substitution at C5 of the thiazolidinedione **16** and thiohydantoin **26** was also poorly tolerated, while both a 5-phenyl or 5-benzyl group on these heterocycles was tolerated, this is consistent with the SAR observed for rhodanines. Finally, trimethadione **28** and dimethadione **29** have no binding to hCA II.

Given that the 3-unsubstituted-2,4-oxazolidinedione fragment is not known as a ZBG in the PDB, we next searched the PDB for protein:ligand crystal structures comprising the other hit fragments (as 3-unsubstituted heterocycles) to see if they are known as metal binding groups. The 2-thioxo-1,3-oxazolidin-4-one fragment of **14′** is not in the PDB. One protein:ligand crystal

structure where the ligand comprises a 3-unsubstituted thiohydantoin fragment as in **27′** is known, PDB ID 1HLF.[49] The ligand in structure 1HLF is glucopyranosylidene-spiro-thiohydantoin, while the protein is glycogen phosphorylase B, not a metalloprotein. Three protein:rhodanine structures, with a 3-unsubstituted rhodanine, as in **24** and **25**, are known, all with the bacterial enzyme MurD ligase, also not a metalloprotein (PDB IDs 2WJP, 2Y68 and 2Y1O).[50-52] There were more than 20 protein:ligand structures in the PDB for the 3-unsubstituted 1,3-thiazolidine-2,4-dione fragment, many with antidiabetic drugs that comprise this fragment, and similarly to the 3-unsubstituted-2,4-oxazolidinedione (**12**) inhibit gamma peroxisome proliferator-activated receptor (γPPAR). Rosiglitazone, an antidiabetic drug within this fragment class appears in eight γPPAR related structures including PDB ID 2PRG.[53] Structures of the antidiabetic drugs pioglitazone and rosiglitazone in complex with monoamine oxidase B (PDB ID 4AZ9[54] and 4A7A[54], respectively) and troglitazone in complex with cytochrome P450 2C8 (PDB ID 2VN0) are also known. Other thiazolidinedione structures are found bound to Pim-1 kinase (PDB ID 3VC4,[55] 3ZW3[56] and PDB ID 4DTK[57]); estrogen related receptor alpha (PDB ID 3K6P); phosphoinositide 3-kinase gamma (PI3Kγ) (PDB ID 2A4Z[58] and 2A5U[56]); CDK2 (PDB ID 2UZO);[59] MurD ligase (PDB ID 2Y66, 2Y67, 2X50 - similar to rhodanine structures with this enzyme mentioned above)[50, 60] and with fatty acid-binding protein 4 (FABP4) (PDB ID 2QM9) – none of which have the fragment bound to a metal ion.[61]

Interestingly, the hydantoin chemotype, although displaying no CA II binding in this study, is known as a ZBG. X-ray crystal structures of a 5-substituted hydantoin with the zinc metalloenzyme, tumour necrosis factor-α (TNF-α) converting enzyme (TACE), have the acidic imide nitrogen of the hydantoin coordinated to the zinc of TACE (PDB IDs 3L0T and 3L0V[62], 3LE9 and 3LEA[63]). Additionally, structures with a disintegrin and metalloproteinase with thrombospondin motifs-4 (ADAMTS-4) (PDB IDs 4WK7, 4WKE, 4WKI) also have the imide

nitrogen of the hydantoin ring interacting directly with the catalytic zinc.[64] Further structures with matrix metalloproteins (MMP) are reported (3UVC with MMP12, 4JPA with MMP13[65]) showing a zinc interaction with the ligand. The zinc in these enzymes is coordinated to three protein histidine residues, the same coordination as found in hCA II.

Collectively the SAR generated in this study confirms the importance of the acidic cyclic imide NH group for the oxazolidinedione and other heterocycles to act as a ZBG. The SAR is however more informative, it demonstrates that the zinc interaction alone is not sufficient for good CA II binding but rather that a interdependent combination of the acidic imide, ring heteroatom (with O > S > NH) and 2-carbonyl/thiocarbonyl group in parallel with the introduction of a flexible 5-substituent contribute to the strength and specificity of CA II binding. We have identified 3-unsubstituted 2,4-oxazolidinedione, 2-thioxo-1,3-oxazolidin-4-one, thiohydantoin and 1,3-thiazolidine-2,4-dione fragments as ZBGs which were not previously known in the PDB. All have potential for CA targeting strategies with new chemical entities. In contrast, the hydantoin chemotype is previously known as a ZBG yet displayed no CA II binding. Together with the SAR of this study, the findings in the PDB indicate that selective targeting of zinc metalloenzymes is possible through a combination of ligand structural features and is not limited solely to the ZBG.

Chemical Synthesis

The synthetic route to 2,4-oxazolidinediones **10** and **11**, 2,4-thiazolidinediones **13** and 2-thioxo-1,3-oxazolidin-4-one **14′** is presented in Scheme 1. Palladium-catalysed Suzuki-Miyaura coupling reaction of the phenyl boronic acids **1a-b** with ethyl glyoxylate generated the precursor mandelic acid ethyl esters **2a-b** in good yield.[66] Condensation of **2a-b** with urea or thiourea in the presence of NaOEt (21 wt.% in ethanol), followed by acidification with HCl

(1.0 N), provided the target oxazolidinediones **10** and **11**, 2,4-thiazolidinediones **13** and 2-thioxo-1,3-oxazolidin-4-one **14′**, respectively.[67]

Scheme 1. Synthesis of oxazolidindione (**10** and **11**), thiazolidinedione (**13**) and 2-thioxo-1,3-oxazolidin-4-one (**14′**) fragments.

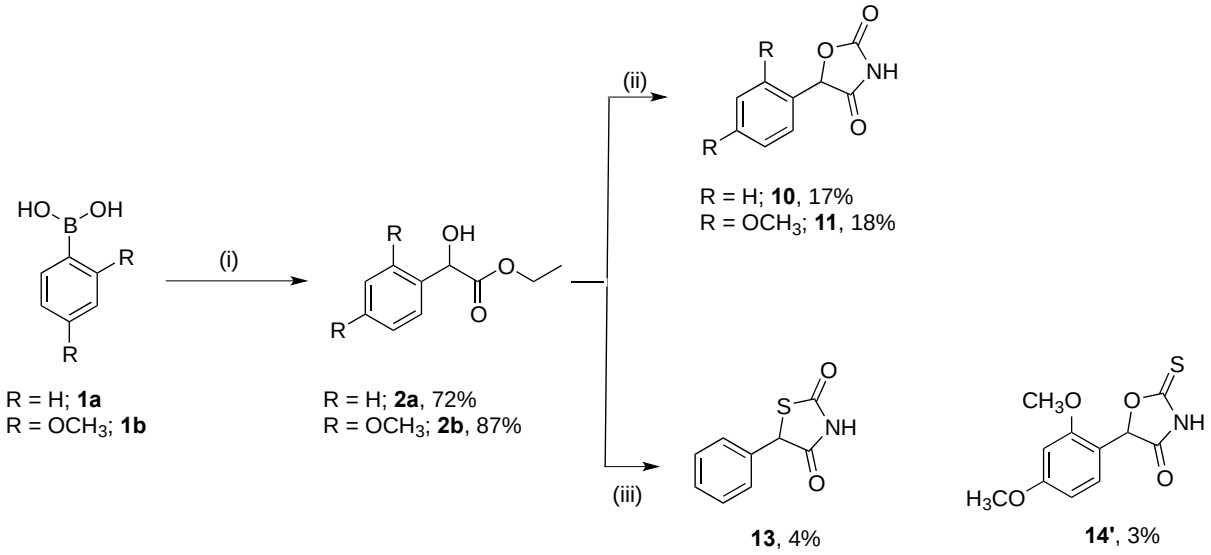

Reagents and conditions: (i) ethyl glyoxylate, $Pd_2(dba)_3.CHCl_3$, 2-(di-tert-butylphosphino)biphenyl, Cs_2CO_3, toluene 80 °C, 4-5 h; (ii) urea, 21 wt. % NaOEt in EtOH, dry EtOH, 0 °C-rt, 30 min, then reflux 3.5 h; (iii) thiourea, 21 wt. % NaOEt in EtOH, dry EtOH, 0 °C-rt 30 min, then reflux 3.5 h.

Benzylidine hydantoins **18** and **19** were synthesised by acid mediated coupling of hydantoin with benzaldehydes **3a-b** followed by hydrolysis, Scheme 2. Reduction of the benzylidine double bond proceeded with Pd-catalysed hydrogenation to provide the related benzyl hydantoins **20** and **21** in good yield, Scheme 2. Thiohydantoin fragment **26** was prepared similarly to **19** from **3b** and thiohydantoin instead of hydantoin, Scheme 2.[68] Attempts to reduce the benzylidine double bond of **26** with Pd/C or $Pd(OH)_2$ catalysed hydrogenation, transfer hydrogenation or 2.0 M $LiBH_4$ in THF resulted in no reaction.[68] The reduction of **26** was

however achieved with Zn-AcOH, affording benzyl thiohydantoin **27** in 65% yield (Scheme 2).[69]

Scheme 2. Synthesis of hydantoin (**18-21**) and thiohydantoin (**26** and **27**) fragments.

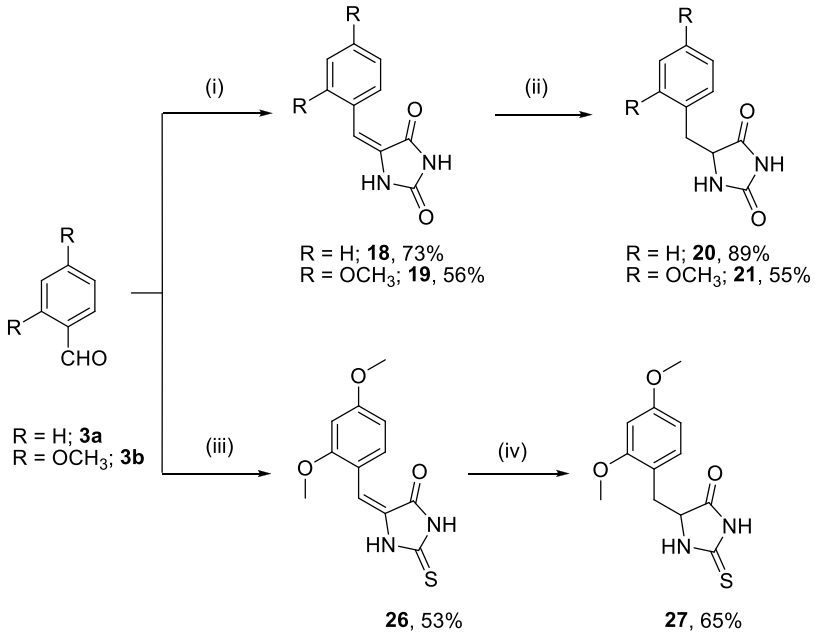

Reagents and conditions: (i) (a) hydantoin, anhyd. NaOAc, AcOH, 170 °C, 3 h; (b) H_2O, rt, overnight; (ii) 10% Pd/C, EtOH, H_2, rt, 5 h; (iii) (a) 2-thiohydantoin, anhyd. NaOAc, AcOH, 170 °C, 3 h; (b) H_2O, rt, overnight; (iv) Zn, AcOH, reflux, overnight.

Benzaldehydes **3a** and **3b** were also the core reagent for the synthesis of thiazolidinediones **16-17** and rhodanines **22-25**. Knoevenagel type condensation of **3a** and **3b** with rhodanine afforded benzylidine rhodanines **22** and **23**, respectively, while reaction of **3b** and 2,4-thiazolidinedione afforded benzylidene thiazolidinedione **16**, Scheme 3.[70] Regiospecific reduction of the benzylidene double bond of **22**, **23** and **16** with 2.0 M $LiBH_4$ in THF provided the corresponding benzyl rhodanines **24** and **25** and benzyl thiazolidinedione **17**, respectively (Scheme 3).[71]

Scheme 3: Synthesis of 2,4-thiazolidinedione (**16-17**) and rhodanine (**22-25**) fragments.

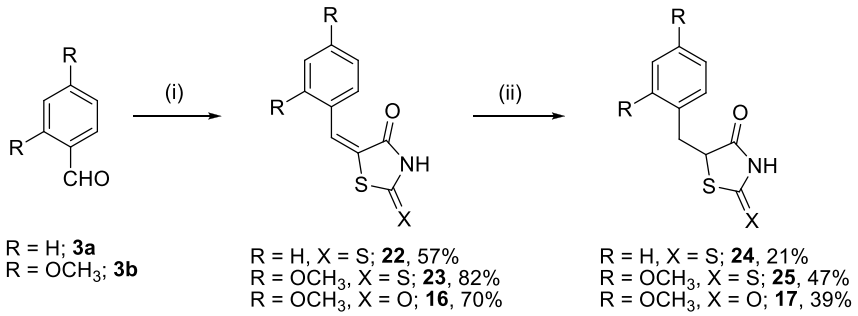

Reagents and conditions: (i) rhodanine (for **22** and **23**) or 2,4-thiazolidinedione (for **16**), NH_4OAc, toluene, reflux, 3 h; (ii) 2.0 M $LiBH_4$ in THF, pyridine-THF, reflux, 5 h; (iii) 2.0 M $LiBH_4$ in THF, pyridine-THF, reflux, 5 h.

Conclusion

Here we have discovered a new zinc binding chemotype, 3-unsubstituted-2,4-oxazolidinedione, with affinity for CA II that is of a magnitude similar to fragment sized primary benzene sulfonamides. A cascade of biophysical screening methods was employed to evaluate binding to CA II, with native state nanoESI-MS evaluated for primary screening, with SPR and protein X-ray crystallography providing validation. We found that nanoESI-MS and SPR provided agreement of both the magnitude and trend of K_D values. The straightforward metric of FA_{MS} appears to offer the opportunity for rapid, semi-quantitative assessment of fragment binding strength using nanoESI-MS as a primary screen in FBDD, while K_D values determined using mass spectrometry provide quantitative data. Both mass spectrometry methods allow fragments to be ranked and prioritised based on affinity for the protein, with the many advantages outlined in our earlier study such as low protein concentration, low fragment concentration (reduces solubility problems), rapid analysis with no need for immobilisation of the protein. Our findings provide support for the relatively untapped opportunity to consider to apply native state mass spectrometry as a complementary fragment screening method to accelerate drug discovery.

Furthermore, SAR by MS[35] was employed and found to be highly suited to establish SAR around the initial hit fragment. Protein X-ray crystallography established that the 3-unsubstituted-2,4-oxazolidinedione fragment bound to CA II via an interaction of the acidic ring nitrogen with the CA II active site zinc, as well as a hydrogen bond between the oxazolidinedione ring oxygen and the CA II protein backbone. A significant finding in relation to SAR was that hydantoins (**15**, **18-21**) had no affinity for CA II, even though the hydantoin heterocycle is known as a zinc binding chemotype with other proteins where the zinc is coordinated to three histidine residues, the same coordination as found in hCA II.[63-65] Together these finding further demonstrate that the fragment-zinc interaction alone is not sufficient for strong CA II binding and that further H-bond interactions between the fragment and CA II are critical. This also indicates that CA II may be selectively targeted over other zinc metalloenzymes, consistent with the findings of CA II binding of the classical primary sulfonamides[9] where the strong binding affinity and specificity of the primary sulfonamide functional group for CA II is attributed to two key hydrogen bonds with the CA II active site residues in addition to the zinc-sulfonamide interaction.[34] To conclude, 3-unsubstituted-2,4-oxazolidinedione, and other heterocycles presented herein, represent new and potentially useful starting points for development of novel and selective CA inhibitors. Additionally, native state mass spectrometry was successfully applied as a primary fragment screen, with successful extension to generate SAR using "fragment SAR by MS".

Experimental

General Chemistry. All reactions were carried out in dry solvents under anhydrous conditions, unless otherwise mentioned. All chemicals were purchased commercially and used without further purification. All reactions were monitored by TLC using silica plates with visualisation of product bands by UV fluorescence (λ = 254 nm) and charring with Vanillin (6 g vanillin in

100 mL of EtOH containing 1% (v/v) concentrated sulfuric acid) stain. Silica gel flash chromatography was performed using silica gel 60 Å (230-400 mesh). NMR (^{1}H, ^{13}C, COSY, HSQC) spectra were recorded on the 500 MHz spectrometer at 25°C. Chemical shifts for ^{1}H and ^{13}C NMR obtained in DMSO-*d*$_6$ are reported in ppm relative to residual solvent proton (δ = 2.50 ppm) and carbon (δ = 39.5 ppm) signals respectively. Multiplicity is indicated as follows: s (singlet), d (doublet), t (triplet), q (quartet), m (multiplet), dd (doublet of doublet), bs (broad signal). Coupling constants are reported in hertz (Hz). High- and low-resolution mass spectra were acquired using electrospray as the ionization technique in positive-ion and/or negative-ion modes as stated. All MS analysis samples were prepared as solutions in methanol. Purity of compounds all compounds was >95% as determined by HPLC instrument (Agilent 1100 series) with UV detection. The melting points are uncorrected. Proton and carbon atoms for NMR assignments are designated as shown in the Supporting Information.

General procedure 1: Suzuki-Miyaura coupling reaction to prepare mandelic esters.

To the appropriate boronic acid **1a** or **1b** (1.5 equiv) and Cs_2CO_3 (1 equiv) suspended in dry toulene at room temperature was added $Pd_2(dba)_3.CHCl_3$ (0.0125 equiv), 2-di-*tert*-butylphoshphanylbiphenyl (0.05 equiv) and ethyl glyoxylate (1.0 equiv) under argon atmosphere. The reaction mixture was stirred at 80 °C for 4-5 h. After completion of reaction (as evidenced by TLC), the reaction was quenched by addition of water (10-15 mL) and extracted with DCM (3 × 20 mL). The combined organic extracts were washed with brine (1 × 15 mL), dried over $MgSO_4$ and concentrated in vacuo. The crude residue was purified by flash chromatography to provide mandelic esters **2a** and **2b**, respectively.

General procedure 2: Synthesis of phenyl-2,4-oxazolidindione and phenyl-2,4-thiazolidinedione fragments.

A sodium ethoxide solution (21 wt. % in ethanol, 1.2 equiv) was cooled to 0 °C and urea (for phenyl-2,4-oxazolidindiones) or thiourea (for phenyl-2,4-thiazolidinediones) added (1 equiv) in one portion followed by dropwise addition of an ice-cold solution of mandelic ester (**2a** or **2b**, 1 equiv) in absolute EtOH (2-3 mL) over 5 min. The reaction mixture was allowed to warm to room temperature over 15-20 min and then refluxed for 3.5 h. EtOH was evaporated under vacuum, the remaining residue was suspended in a mixture of water (6 mL) and Et_2O (4 mL), acidified with 1N HCl (to pH 2-4) and extracted with Et_2O (2 × 15 mL). The combined organic extracts were washed with brine (1 × 10 mL), dried over $MgSO_4$ and concentrated in vacuo. The crude residue was purified by flash chromatography to provide fragments **10**-**11**, **13** and **14′**.

General procedure 3: Synthesis of hydantoin and thiohydantoin fragments

Hydantoin (1.1 equiv) was added to a solution of glacial acetic acid (0.33 mL/mmol) and acetic anhydride (0.044 mL/mmol) under argon atmosphere, followed by addition of anhydrous NaOAc (2 equiv), and benzaldehyde **3a** or **3b** (1 equiv). The resulting mixture was stirred at 170 °C under an argon atmosphere. After 3 h, the reaction mixture was cooled to 110 °C, water was added and the mixture was stirred overnight at room temperature. The precipitate that formed was collected by filtration, washed with water (4 × 20 mL) and purified by flash chromatography to provide the desired fragments **18** and **19**. Fragment **26** was prepared similarly from 2-thiohydantoin (1.1 equiv) and benzaldehyde **3b**.

General procedure 4: Synthesis of 5-benzylimidazoline-2,4-dione (hydantoin) fragments.

To a solution of **18** or **19** (1 equiv) in absolute EtOH was added Pd/C (40% by weight of **18** or **19**). The reaction mixture was stirred at room temperature overnight under an atmosphere of hydrogen. After completion of reaction (as evidenced by TLC), the reaction mixture was

filtered through celite and the celite washed with MeOH (15-20 mL). The solvent was evaporated in vacuo and the crude residue purified by flash chromatography to provide the fragments **20** and **21**.

General procedure 5: Synthesis of 5-benzylidenethiazolidine-2,4-dione or 5-benzylidene-2-sulfanylidene-1,3-thiazolidin-4-one (thiazolidinedione and rhodanine) fragments.

To an appropriate benzaldehyde **3a** or **3b** (1 equiv) in dry toulene (10-15 mL) at room temperature, was added rhodanine (1 equiv) or 2,4-thiazolidinedione (1 equiv) and anhydrous ammonium acetate (1.5 equiv) under argon atmosphere. The resultant reaction mixture stirred at 90-100 °C for 3 h. After 3 h, the precipitate of the desired product was filtered and washed with Et_2O (2 × 15 mL). The crude solid was recrystallised in absolute EtOH to provide the desired compounds as described in the series of **16** and **22-23**.

General procedure 6: Synthesis of 5-benzyl-2-sulfanylidene-1,3-thiazolidin-4-one or 5-Benzylthiazolidine-2,4-dione (thiazolidinedione and rhodanine) fragments.

To a stirred solution of appropriate compound **16** or **22** or **23** (1 equiv) in dry pyridine (0.81 mL/mmol) and dry THF (0.66 mL/mmol), was added 2.0 M $LiBH_4$ in THF (2.2 equiv) at room temperature and under argon atmosphere (Effervescences were controlled by addition rate of $LiBH_4$ solution). The resulting mixture was refluxed for 3-4 h. After completion of reaction (as evidenced by TLC), the reaction mixture was quenched by 1N HCl (1-2 mL), extracted with EtOAc (3 × 15 mL). The combined organic layers were washed with brine (1 × 10 mL), dried over $MgSO_4$ and concentrated in vacuo. The crude residue was purified by flash chromatography to provide the desired compounds as described in the series of **17** and **24-25**.

Ethyl 2-hydroxy-2-phenylacetate (2a)[66]

Compound **2a** was synthesized from ethyl glyoxylate 50% solution in toulene (0.59 mL, 3.0 mmol) and compound **1a** (0.548 g, 4.50 mmol) according to general procedure 1. The crude residue was purified by flash chromatography (Gradient: 8−10 % EtOAc in *n*-hexane) to afford the title compound as a colorless oil (0.394 g, 72.96%). R_f = 0.46 (30% EtOAc in *n*-hexane). ^{1}H NMR (500 MHz, $CDCl_3$) δ_H = 7.43-7.41 (m, 2H, H_{Ar}), 7.38-7.35 (m, 2H, H_{Ar}), 7.34-7.31 (m, 1H, H_{Ar}), 5.16 (d, *J* = 5.25 Hz, 1H, OH-C<u>H</u>), 4.30-4.24 (m, 1H, C<u>H</u>H-CH_3), 4.21-4.14 (m, 1H, CH<u>H</u>-CH_3), 3.47 (d, *J* = 5.7 Hz, 1H, CH-O<u>H</u>), 1.23 (t, *J* = 7.15 Hz, 3H, CH_2-C<u>H</u>$_3$), general assignments were confirmed by ^{1}H-^{1}H gCOSY. ^{13}C NMR (125 MHz, $CDCl_3$) δ_C = 173.8 (C=O), 138.6 (C_{quat}), 128.7 (2 × CH_{Ar}), 128.5 (CH_{Ar}), 126.7 (2 × CH_{Ar}), 73.0 (OH-CH), 62.4 (<u>C</u>H_2-CH_3), 14.2 (CH_2-<u>C</u>H_3), general assignments were confirmed by ^{1}H-^{13}C HSQC. LRMS-ESI: *m/z* = 203 $[M + Na]^+$.

Ethyl 2-(2,4-dimethoxyphenyl)-2-hydroxyacetate (2b)[66, 72]

The compound **2b** was synthesized from ethyl glyoxylate 50% solution in toulene (0.19 mL, 1.0 mmol) and compound **1a** (0.272 g, 1.5 mmol) according to general procedure 1. The crude residue was purified by flash chromatography (Gradient: 8−10% EtOAc in *n*-hexane) to afford the title compound as a pale yellow oil (0.209 g, 87.08%). R_f = 0.39 (30% EtOAc in *n*-hexane). ^{1}H NMR (500 MHz, DMSO-d_6) δ_H = 7.20 (d, *J* = 8.4 Hz, 1H, H_{Ar}), 6.54 (d, J_{meta} = 2.4 Hz, 1H, H_{Ar}), 6.51 (dd, $J_{ortho,\ meta}$ = 8.35, 2.4 Hz, 1H, H_{Ar}), 5.66 (d, *J* = 6.05 Hz, 1H, OH-C<u>H</u>), 5.20 (d, *J* = 6.05 Hz, 1H, CH-O<u>H</u>), 4.09-4.02 (m, 2H, C<u>H</u>$_2$-CH_3), 3.75 (s, 6H, 2 × OCH_3), 1.12 (t, *J* = 7.1 Hz, 3H, CH_2-C<u>H</u>$_3$), general assignments were confirmed by ^{1}H-^{1}H gCOSY. ^{13}C NMR (125 MHz, DMSO-d_6) δ_C = 172.9 (C=O), 160.3 (C_{quat}), 157.4 (C_{quat}), 128.7 (CH_{Ar}), 120.6 (C_{quat}), 104.7 (CH_{Ar}), 98.3 (CH_{Ar}), 66.9 (OH-CH), 60.0 (<u>C</u>H_2-CH_3), 55.5 (OCH_3), 55.2 (OCH_3), 14.1 (CH_2-<u>C</u>H_3), general assignments were confirmed by ^{1}H-^{13}C HSQC. LRMS-ESI: *m/z* = 263 $[M + Na]^+$.

5-Phenyl-1,3-oxazolidine-2,4-dione (10)

The compound **10** was synthesized from compound **2a** (0.179 g, 0.9944 mmol) according to general procedure 2. The crude residue was purified by flash chromatography (Gradient: 15−20% EtOAc in *n*-hexane) to afford the title compound as a white solid (0.030 g, 17.04%). R_f = 0.34 (30% EtOAc in *n*-hexane). Mp = 100−102°C. ^{1}H NMR (500 MHz, DMSO-d_6) δ_H = 12.15 (s, 1H, NH), 7.46-7.44 (m, 3H, H_{Ar}), 7.41-7.40 (m, 2H, H_{Ar}), 6.04 (s, 1H, O-CH-CO), general assignments were confirmed by ^{1}H-^{1}H gCOSY. ^{13}C NMR (125 MHz, DMSO-d_6) δ_C = 173.5 (C=O), 155.6 (C=O), 132.8 (C_{quat}), 129.5 (CH_{Ar}), 128.9 (2 × CH_{Ar}), 126.8 (2 × CH_{Ar}), 81.0 (O-CH-CO), general assignments were confirmed by ^{1}H-^{13}C HSQC. LRMS-ESI: *m/z* = 176 $[M - H]^+$. HRMS-ESI: $[M - H]^+$ calcd for $C_9H_6NO_3$, 176.0342, found 176.0352.

5-(2,4-Dimethoxyphenyl)-1,3-oxazolidine-2,4-dione (11)

The compound **11** was synthesized from compound **2b** (0.19 g, 0.7908 mmol) according to general procedure 2. The crude residue was purified by flash chromatography (Gradient: 4−5% MeOH in DCM) to afford the title compound as a white solid (0.035 g, 18.71%). R_f = 0.58 (10% MeOH in DCM). Mp = 180−182°C. ^{1}H NMR (500 MHz, DMSO-d_6) δ_H = 11.86 (s, 1H, NH), 7.29 (d, J_{ortho} = 8.4 Hz, 1H, H_{Ar}), 6.63 (d, J_{meta} = 2.35 Hz, 1H, H_{Ar}), 6.56 (dd, $J_{ortho,\ meta}$ = 8.4, 2.4 Hz, 1H, H_{Ar}), 5.89 (s, 1H, O-CH-CO), 3.79 (s, 3H, OCH_3), 3.74 (s, 3H, OCH_3), general assignments were confirmed by ^{1}H-^{1}H gCOSY. ^{13}C NMR (125 MHz, DMSO-d_6) δ_C = 174.3 (C=O), 162.4 (C=O), 159.3 (C_{quat}), 155.9 (C_{quat}), 132.9 (CH_{Ar}), 112.8 (C_{quat}), 105.1 (CH_{Ar}), 99.1 (CH_{Ar}), 79.8 (O-CH-CO), 55.9 (OCH_3), 55.5 (OCH_3), general assignments were confirmed by ^{1}H-^{13}C HSQC. LRMS-ESI: *m/z* = 236 $[M - H]^+$. HRMS-ESI: $[M + Na]^+$ calcd for $C_{11}H_{11}NNaO_5$, 260.0529, found 260.0529.

5-Phenyl-1,3-thiazolidine-2,4-dione (13)

The compound **13** was synthesized from compound **2a** (0.45 g, 2.5 mmol) according to general procedure 2. The crude residue was purified by flash chromatography (gradient: 10−15% EtOAc in *n*-hexane) to afford the title compound as a white solid (0.020 g, 4.14%). R_f = 0.37 (30% EtOAc in *n*-hexane). Mp = 134−136°C. ^{1}H NMR (500 MHz, DMSO-*d*$_6$) δ_H = 13.55 (s, 1H, NH), 7.49-7.47 (m, 3H, H_{Ar}), 7.38-7.36 (m, 2H, H_{Ar}), 6.27 (s, 1H, S-CH-CO), general assignments were confirmed by ^{1}H-^{1}H gCOSY. ^{13}C NMR (125 MHz, DMSO-*d*$_6$) δ_C = 192.1 (C=O), 174.7 (C=O), 132.5 (C_{quat}), 130.3 (CH_{Ar}), 129.7 (2 × CH_{Ar}), 127.5 (2 × CH_{Ar}), 84.8 (S-CH-CO), general assignments were confirmed by ^{1}H-^{13}C HSQC. LRMS-ESI: *m/z* = 192 [M − H]$^+$. HRMS-ESI: [M − H]$^+$ calcd for $C_9H_6NO_2S$, 192.0114, found 192.0127.

5-(2,4-Dimethoxyphenyl)-2-thioxo-1,3-oxazolidin-4-one (14′)

The compound **14'** was synthesized from compound **2b** (0.385 g, 1.604 mmol) according to general procedure 2. The crude residue was purified by flash chromatography (gradient: 10−20% EtOAc in *n*-hexane) to afford the title compound as a colorless oil (0.013 g, 3.20%). ^{1}H NMR (500 MHz, DMSO-*d*$_6$) δ_H = 13.25 (s, 1H, NH), 7.31 (d, *J* = 8.45 Hz, 1H, H_{Ar}), 6.65 (d, *J* = 2.35 Hz, 1H, H_{Ar}), 6.59 (dd, *J* = 8.35, 2.4 Hz, 1H, H_{Ar}), 6.10 (s, 1H, O-CH-CO), 3.80 (s, 3H, OCH_3), 3.74 (s, 3H, OCH_3). ^{13}C NMR (125 MHz, DMSO-*d*$_6$) δ_C = 173.03 (C=O), 160.4 (C=S), 157.5 (C_{quat}), 128.8 (CH_{Ar}), 120.6 (CH_{Ar}), 112.2 (C_{quat}), 104.8 (CH_{Ar}), 98.4 (C_{quat}), 83.1 (O-CH-CO), 55.6 (OCH_3), 55.3 (OCH_3). LRMS-ESI: *m/z* = 252 [M − H]$^+$.

5-(Phenylmethylidene)imidazolidine-2,4-dione (18)

The compound **18** was synthesized from compound **3a** (1.0 g, 9.423 mmol) according to general procedure 3. The crude residue was purified by flash chromatography (Gradient: 20−25% EtOAc in *n*-hexane) to afford the title compound as a yellow solid (1.30 g, 73.44 %). R_f = 0.17

(30% EtOAc in *n*-hexane). Mp = 270−275°C, decomposition. ^{1}H NMR (500 MHz, DMSO-d_6) δ_H = 7.61 (d, J_{ortho} = 7.25 Hz, 2H, H_{Ar}), 7.37 (t, J_{ortho} = 7.85 Hz, 2H, H_{Ar}), 7.30-7.27 (m, 1H, H_{Ar}), 6.30 (s, 1H, Ph-CH=C), NH protons are in exchange, general assignments were confirmed by ^{1}H-^{1}H gCOSY. ^{13}C NMR (125 MHz, DMSO-d_6) δ_C = 165.9 (C=O), 156.0 (C=O), 133.1 (C_{quat}), 129.5 (2 × CH_{Ar}), 129.0 (2 × CH_{Ar}), 128.6 (CH_{Ar}), 128.2 (C_{quat}), 108.5 (Ph-CH=C), general assignments were confirmed by ^{1}H-^{13}C HSQC. LRMS-ESI: *m/z* = 189 $[M + H]^+$. HRMS-ESI: $[M + Na]^+$ calcd for $C_{10}H_8N_2NaO_2$, 211.0478, found 211.0477.

5-[(2,4-Dimethoxyphenyl)methylidene]imidazolidine-2,4-dione (19)

The compound **19** was synthesized from compound **3b** (1.0 g, 6.0175 mmol) according to general procedure 3. The crude residue was purified by flash chromatography (Gradient: 60−80% EtOAc in *n*-hexane) to afford the title compound as a yellow solid (0.850 g, 56.97%). R_f = 0.55 (50% EtOAc in *n*-hexane). Mp = 230−232°C. ^{1}H NMR (500 MHz, DMSO-d_6) δ_H = 7.56 (d, J_{ortho} = 8.45 Hz, 1H, H_{Ar}), 6.61-6.60 (m, 2H, H_{Ar} and Ph-CH-C), 6.55 (d, J_{ortho} = 8.30 Hz, 1H, H_{Ar}), 3.84 (s, 3H, OCH_3), 3.81 (s, 3H, OCH_3), NH protons are in exchange, general assignments were confirmed by ^{1}H-^{1}H gCOSY. ^{13}C NMR (125 MHz, DMSO-d_6) δ_C = 166.1 (C=O), 161.6 (C=O), 159.1 (C_{quat}), 156.0 (C_{quat}), 130.6 (CH_{Ar}), 126.5 (C_{quat}), 114.7 (C_{quat}), 106.0 (CH_{Ar}), 103.5 (CH_{Ar}), 98.7 (Ph-CH=C), 56.2 (OCH_3), 55.9 (OCH_3), general assignments were confirmed by ^{1}H-^{13}C HSQC. LRMS-ESI: *m/z* = 249 $[M + H]^+$. HRMS-ESI: $[M + H]^+$ calcd for $C_{12}H_{13}N_2O_4$, 249.0870, found 249.0869.

5-Benzylimidazolidine-2,4-dione (20)

The compound **20** was synthesized from compound **18** (0.1 g, 0.5317 mmol) according to general procedure 4. The crude residue was purified by flash chromatography (Gradient: 50−60% EtOAc in *n*-hexane) to afford the title compound as a white solid (0.09 g, 89.10%). R_f

= 0.17 (50% EtOAc in *n*-hexane). Mp = 191−193°C. ^{1}H NMR (500 MHz, DMSO-d_6) δ_H = 10.43 (s, 1H, NH), 7.91 (s, 1H, NH), 7.29-7.26 (m, 2H, H_{Ar}), 7.23-7.21 (m, 1H, H_{Ar}), 7.19-7.18 (m, 2H, H_{Ar}), 4.32 (t, J = 5.85 Hz, 1H, Ph-CH_2-C<u>H</u>), 2.97-2.93 (m, 1H, Ph-C<u>H</u>H-CH), 2.93-2.89 (m, 1H, Ph-CH<u>H</u>-CH), general assignments were confirmed by ^{1}H-^{1}H gCOSY. ^{13}C NMR (125 MHz, DMSO-d_6) δ_C = 175.2 (C=O), 156.2 (C=O), 135.6 (C_{quat}), 129.7 (2 × CH_{Ar}), 128.1 (2 × CH_{Ar}), 126.6 (CH_{Ar}), 58.4 (Ph-CH_2-<u>C</u>H), 36.4 (Ph-<u>C</u>H_2-CH), general assignments were confirmed by ^{1}H-^{13}C HSQC. LRMS-ESI: *m/z* = 191 $[M + H]^+$, 213 $[M + Na]^+$. HRMS-ESI: $[M + Na]^+$ calcd for $C_{10}H_{10}N_2NaO_2$, 213.0635, found 213.0634.

5-[(2,4-Dimethoxyphenyl)methyl]imidazolidine-2,4-dione (21)

The compound **21** was synthesized from compound **19** (0.1 g, 0.4030 mmol) according to general procedure 4. The crude residue was purified by flash chromatography (Gradient: 30−40% EtOAc in *n*-hexane) to afford the title compound as a white solid (0.055 g, 55.0%). R_f = 0.13 (50% EtOAc in *n*-hexane). Mp = 165−167°C. ^{1}H NMR (500 MHz, DMSO-d_6) δ_H = 10.49 (s, 1H, NH), 7.69 (s, 1H, NH), 7.02 (d, J_{ortho} = 8.25 Hz, 1H, H_{Ar}), 6.52 (d, J_{meta} = 2.4 Hz, 1H, H_{Ar}), 6.44 (dd, $J_{ortho,\ meta}$ = 8.3, 2.4 Hz, 1H, H_{Ar}), 4.19-4.16 (m, 1H, Ph-CH_2-C<u>H</u>), 3.75 (s, 3H, OCH_3), 3.74 (s, 3H, OCH_3), 2.98 (dd, J = 13.9, 4.95 Hz, 1H, Ph-C<u>H</u>H-CH), 2.65 (dd, J = 13.9, 7.45 Hz, 1H, Ph-CH<u>H</u>-CH), general assignments were confirmed by ^{1}H-^{1}H gCOSY. ^{13}C NMR (125 MHz, DMSO-d_6) δ_C = 175.5 (C=O), 159.6 (C=O), 158.3 (C_{quat}), 157.3 (C_{quat}), 131.3 (CH_{Ar}), 116.4 (C_{quat}), 104.4 (CH_{Ar}), 98.2 (CH_{Ar}), 57.6 (Ph-CH_2-<u>C</u>H), 55.4 (OCH_3), 55.1 (OCH_3), 31.6 (Ph-<u>C</u>H_2-CH), general assignments were confirmed by ^{1}H-^{13}C HSQC. LRMS-ESI: *m/z* = 251 $[M + H]^+$, 273 $[M + Na]^+$. HRMS-ESI: $[M + Na]^+$ calcd for $C_{12}H_{14}N_2NaO_4$, 273.0846, found 273.0845.

5-[(2,4-Dimethoxyphenyl)methylidene]-2-sulfanylideneimidazolidin-4-one (26)

The compound **26** was synthesized from compound **3b** (1.0 g, 6.0175 mmol) according to general procedure 3. The crude residue was purified by flash chromatography (Gradient: 10−20% EtOAc in *n*-hexane) to afford the title compound as a yellow solid (0.852 g, 53.52%). R_f = 0.25 (30% EtOAc in *n*-hexane). Mp = 235−237°C. ^{1}H NMR (500 MHz, DMSO-d_6) δ_H = 12.23 (s, 1H, NH), 11.93 (s, 1H, NH), 7.74 (d, J_{ortho} = 8.65 Hz, 1H, H_{Ar}), 6.69 (s, 1H, Ph-CH=C), 6.61 (d, J_{meta} = 2.35 Hz, 1H, H_{Ar}), 6.58 (dd, $J_{ortho,\ meta}$ = 8.6, 2.4 Hz, 1H, H_{Ar}), 3.86 (s, 3H, OCH_3), 3.83 (s, 3H, OCH_3), general assignments were confirmed by ^{1}H-^{1}H gCOSY. ^{13}C NMR (125 MHz, DMSO-d_6) δ_C = 178.1 (C=S), 165.8 (C=O), 162.1 (C_{quat}), 159.2 (C_{quat}), 131.3 (CH_{Ar}), 125.8 (C_{quat}), 113.7 (C_{quat}), 106.5 (Ph-CH=C), 105.9 (CH_{Ar}), 98.2 (CH_{Ar}), 55.9 (OCH_3), 55.5 (OCH_3), general assignments were confirmed by ^{1}H-^{13}C HSQC. LRMS-ESI: *m/z* = 265 $[M + H]^+$, 287 $[M + Na]^+$. HRMS (ESI): $[M + H]^+$ calcd for $C_{12}H_{13}N_2O_3S$, 265.0641, found 265.0641.

5-[(2,4-Dimethoxyphenyl)methyl]-2-sulfanylideneimidazolidin-4-one (27)

To 5-benzylidene-2-sulfanylideneimidazolidin-4-one **26** (0.1 g, 0.3787 mmol) in glacial acetic acid (2 mL) was added Zn dust (0.272 g, 4.1657 mmol) at room temperature. The resultant reaction mixture was refluxed for 12-18 h. After completion of reaction (TLC), the reaction mixture was cooled down to 50 °C, added MeOH (5 × acetic acid qty.) refluxed for 5-10 min. The reaction mixture was then filtered through celite bed, washed with MeOH (15-20 mL) and evaporated in vacuo. The crude residue was purified by flash chromatography (Gradient: 15−30% EtOAc in *n*-hexane) to afford the title compound as a yellow solid (0.065 g, 65.0%). R_f = 0.58 (50% EtOAc in *n*-hexane). Mp = 153−155°C. ^{1}H NMR (500 MHz, DMSO-d_6) δ_H = 11.50 (s, 1H, NH), 9.86 (s, 1H, NH), 7.01 (d, J_{ortho} = 8.3 Hz, 1H, H_{Ar}), 6.51 (d, J_{meta} = 2.4 Hz, 1H, H_{Ar}), 6.43 (dd, $J_{ortho,\ meta}$ = 8.3, 2.45 Hz, 1H, H_{Ar}), 4.40-4.38 (m, 1H, Ph-CH_2-CH), 3.76 (s, 3H, OCH_3), 3.74 (s, 3H, OCH_3), 2.96 (dd, *J* = 14.05, 5.65 Hz, 1H, Ph-CHH-CH), 2.78 (dd, *J* =

14.05, 6.65 Hz, 1H, Ph-CHH-CH), general assignments were confirmed by ^{1}H-^{1}H gCOSY. ^{13}C NMR (125 MHz, DMSO-d_6) δ_C = 182.3 (C=S), 176.0 (C=O), 159.8 (C_{quat}), 158.4 (C_{quat}), 131.5 (CH_{Ar}), 115.7 (C_{quat}), 104.5 (CH_{Ar}), 98.3 (CH_{Ar}), 60.7 (Ph-CH_2-CH), 55.5 (OCH_3), 55.2 (OCH_3), 30.8 (Ph-CH_2-CH), general assignments were confirmed by ^{1}H-^{13}C HSQC. LRMS-ESI: *m/z* = 267 $[M + H]^+$, 289 $[M + Na]^+$. HRMS-ESI: $[M + H]^+$ calcd for $C_{12}H_{15}N_2O_3S$, 267.0798, found 267.0798. Compound **27′** was subsequently identified as a ~5% impurity in **27**.

5-(Phenylmethylidene)-2-sulfanylidene-1,3-thiazolidin-4-one (22)

The compound **22** was synthesized from compound **3a** (0.5 g, 4.7116 mmol) according to general procedure 5. The crude residue was recrystallised from EtOH to afford the title compound as a yellow solid (0.6 g, 57.63%). R_f = 0.54 (30% EtOAc in *n*-hexane). Mp = 204−206°C. ^{1}H NMR (500 MHz, DMSO-d_6) δ_H = 13.84 (s, 1H, NH), 7.64 (s, 1H, Ph-CH=C), 7.60-7.59 (m, 2H, H_{Ar}), 7.55-7.48 (m, 3H, H_{Ar}), general assignments were confirmed by ^{1}H-^{1}H gCOSY. ^{13}C NMR (125 MHz, DMSO-d_6) δ_C = 195.7 (C=S), 169.4 (C=O), 133.0 (C_{quat}), 131.6 (Ph-CH=C), 130.7 (CH_{Ar}), 130.5 (2 × CH_{Ar}), 129.4 (2 × CH_{Ar}), 125.5 (C_{quat}), general assignments were confirmed by ^{1}H-^{13}C HSQC. LRMS-ESI: *m/z* = 220 $[M - H]^+$. HRMS-ESI: $[M - H]^+$ calcd for $C_{10}H_6NOS_2$, 219.9885, found 219.9897.

5-[(2,4-Dimethoxyphenyl)methylidene]-2-sulfanylidene-1,3-thiazolidin-4-one (23)

The compound **23** was synthesized from compound **3b** (0.5 g, 3.008 mmol) according to general procedure 5. The crude residue was recrystallised from EtOH to afford the title compound as a yellow solid (0.7 g, 82.84%). R_f = 0.31 (30% EtOAc in *n*-hexane). Mp = 273−275°C, decomposition. ^{1}H NMR (500 MHz, DMSO-d_6) δ_H = 13.65 (s, 1H, NH), 7.74 (s, 1H, Ph-CH=C), 7.33 (d, J_{ortho} = 8.65 Hz, 1H, H_{Ar}), 6.71 (dd, $J_{ortho,\ meta}$ = 8.65, 2.3Hz, 1H, H_{Ar}), 6.68 (s,

1H, H_{Ar}), 3.90 (s, 3H, OCH_3), 3.85 (s, 3H, OCH_3), general assignments were confirmed by ^{1}H-^{1}H gCOSY. ^{13}C NMR (125 MHz, DMSO-d_6) δ_C = 195.8 (C=S), 169.5 (C=O), 163.6 (C_{quat}), 160.0 (C_{quat}), 131.4 (CH_{Ar}), 127.0 (Ph-CH=C), 121.7 (C_{quat}), 114.3 (C_{quat}), 106.9 (CH_{Ar}), 98.6 (CH_{Ar}), 55.9 (OCH_3), 55.7 (OCH_3), general assignments were confirmed by ^{1}H-^{13}C HSQC. LRMS-ESI: *m/z* = 280 $[M - H]^+$. HRMS-ESI: $[M - H]^+$ calcd for $C_{12}H_{10}NO_3S_2$, 280.0097, found 280.0107.

5-Benzyl-2-sulfanylidene-1,3-thiazolidin-4-one (24)

The compound **24** was synthesized from compound **22** (0.1 g, 0.4524 mmol) according to general procedure 6. The crude residue was purified by flash chromatography (Gradient: 15−20% EtOAc in *n*-hexane) to afford the title compound as a white solid (0.021 g, 21.0 %). R_f = 0.34 (30% EtOAc in *n*-hexane). Mp = 119−121°C. ^{1}H NMR (500 MHz, DMSO-d_6) δ_H = 13.16 (s, 1H, NH), 7.33-7.23 (m, 5H, H_{Ar}), 5.04 (dd, *J* = 8.9, 4.6 Hz, 1H, Ph-CH_2-CH), 3.37 (dd, *J* = 14.1, 4.45 Hz, 1H, Ph-CHH-CH), 3.17 (dd, *J* = 14.1, 9.1 Hz, 1H, Ph-CHH-CH), general assignments were confirmed by ^{1}H-^{1}H gCOSY. ^{13}C NMR (125 MHz, DMSO-d_6) δ_C = 203.3 (C=S), 177.9 (C=O), 136.6 (C_{quat}), 129.2 (2 × CH_{Ar}), 128.5 (2 × CH_{Ar}), 127.1 (CH_{Ar}), 55.7 (Ph-CH_2-CH), 36.5 (Ph-CH_2-CH), general assignments were confirmed by ^{1}H-^{13}C HSQC. LRMS-ESI: *m/z* = 222 $[M - H]^+$. HRMS-ESI: $[M - H]^+$ calcd for $C_{10}H_8NOS_2$, 222.0042, found 222.0054.

5-[(2,4-Dimethoxyphenyl)methyl]-2-sulfanylidene-1,3-thiazolidin-4-one (25)

The compound **25** was synthesized from compound **23** (0.2 g, 0.7117 mmol) according to general procedure 6. The crude residue was purified by flash chromatography (Gradient: 12−15% EtOAc in *n*-hexane) to afford the title compound as a yellow solid (0.095 g, 47.26%). R_f = 0.53 (30% EtOAc in *n*-hexane). Mp = 160−162°C. ^{1}H NMR (500 MHz, DMSO-d_6) δ_H =

13.15 (s, 1H, NH), 7.04 (d, J_{ortho} = 8.25 Hz, 1H, H_{Ar}), 6.54 (d, J_{meta} = 2.4 Hz, 1H, H_{Ar}), 6.46 (dd, $J_{ortho,\ meta}$ = 8.3, 2.4 Hz, 1H, H_{Ar}), 4.90 (dd, *J* = 9.6, 4.85 Hz, 1H, Ph-CH_2-C<u>H</u>), 3.77 (s, 3H, OCH_3), 3.74 (s, 3H, OCH_3), 3.36 (dd, *J* = 13.95, 4.85 Hz, 1H, Ph-C<u>H</u>H-CH), 2.95 (dd, *J* = 14.0, 9.6 Hz, 1H, Ph-CH<u>H</u>-CH), general assignments were confirmed by ^{1}H-^{1}H gCOSY. ^{13}C NMR (125 MHz, DMSO-*d*$_6$) δ_C = 203.6 (C=S), 178.2 (C=O), 160.0 (C_{quat}), 158.1 (C_{quat}), 130.8 (CH_{Ar}), 116.9 (C_{quat}), 104.6 (CH_{Ar}), 98.4 (CH_{Ar}), 55.4 (OCH_3), 55.2 (OCH_3), 54.8 (Ph-CH_2-<u>C</u>H), 31.6 (Ph-<u>C</u>H_2-CH), general assignments were confirmed by ^{1}H-^{13}C HSQC. LRMS-ESI: *m/z* = 282 $[M - H]^+$. HRMS-ESI: $[M - H]^+$ calcd for $C_{12}H_{12}NO_3S_2$, 282.0253, found 282.0263.

5-[(2,4-Dimethoxyphenyl)methylidene]-1,3-thiazolidine-2,4-dione (16)

The compound **16** was synthesized from compound **3b** (0.5 g, 3.008 mmol) according to general procedure 5. The crude residue was recrystallised from EtOH to afford the title compound as a yellow solid (0.56 g, 70.26%). R_f = 0.60 (30% EtOAc in *n*-hexane). Mp = 240−242°C, decomposition. ^{1}H NMR (500 MHz, DMSO-*d*$_6$) δ_H = 12.43 (s, 1H, NH), 7.92 (s, 1H, Ph-CH=C), 7.33 (d, J_{ortho} = 8.6 Hz, 1H, H_{Ar}), 6.70 (dd, $J_{ortho,\ meta}$ = 8.65, 2.35 Hz, 1H, H_{Ar}), 6.67 (d, J_{meta} = 2.25 Hz, 1H, H_{Ar}), 3.89 (s, 3H, OCH_3), 3.84 (s, 3H, OCH_3), general assignments were confirmed by ^{1}H-^{1}H gCOSY. ^{13}C NMR (125 MHz, DMSO-*d*$_6$) δ_C = 168.2 (C=O), 167.6 (C=O), 163.1 (C_{quat}), 159.8 (C_{quat}), 130.1 (CH_{Ar}), 126.5 (Ph-<u>C</u>H=C), 119.9 (C_{quat}), 114.3 (C_{quat}), 106.5 (CH_{Ar}), 98.6 (CH_{Ar}), 55.9 (OCH_3), 55.6 (OCH_3), general assignments were confirmed by ^{1}H-^{13}C HSQC. LRMS-ESI: *m/z* = 266 $[M + H]^+$, 288 $[M + Na]^+$. HRMS-ESI: $[M + H]^+$ calcd for $C_{12}H_{12}NO_4S$, 266.0482, found 266.0481.

5-[(2,4-Dimethoxyphenyl)methyl]-1,3-thiazolidine-2,4-dione (17)

The compound **17** was synthesized from compound **16** (0.15 g, 0.5659 mmol) according to general procedure 6. The crude residue was purified by flash chromatography (Gradient:

15−20% EtOAc in *n*-hexane) to afford the title compound as (0.060 g, 39.73%). R_f = 0.33 (30% EtOAc in *n*-hexane). Mp = 169−171°C. ^{1}H NMR (500 MHz, DMSO-d_6) δ_H = 12.01 (s, 1H, NH), 7.04 (d, J_{ortho} = 8.3 Hz, 1H, H_{Ar}), 6.54 (d, J_{meta} = 2.4 Hz, 1H, H_{Ar}), 6.46 (dd, $J_{ortho,\ meta}$ = 8.3, 2.4 Hz, 1H, H_{Ar}), 4.78 (dd, *J* = 10.0, 4.55 Hz, 1H, Ph-CH_2-C<u>H</u>), 3.78 (s, 3H, OCH_3), 3.74 (s, 3H, OCH_3), 3.40 (dd, *J* = 13.9, 4.5 Hz, 1H, Ph-C<u>H</u>H-CH), 2.87 (dd, *J* = 13.9, 10.0 Hz, 1H, Ph-CH<u>H</u>-CH), general assignments were confirmed by ^{1}H-^{1}H gCOSY. ^{13}C NMR (125 MHz, DMSO-d_6) δ_C = 175.9 (C=O), 171.8 (C=O), 159.9 (C_{quat}), 158.2 (C_{quat}), 130.8 (CH_{Ar}), 117.1 (C_{quat}), 104.5 (CH_{Ar}), 98.4 (CH_{Ar}), 55.4 (OCH_3), 55.1 (OCH_3), 51.8 (Ph-CH_2-<u>C</u>H), 32.2 (Ph-<u>C</u>H_2-CH), general assignments were confirmed by ^{1}H-^{13}C HSQC. LRMS-ESI: *m/z* = 268[M + H]$^+$, 290 [M + Na]$^+$. HRMS-ESI: [M + Na]$^+$ calcd for $C_{12}H_{13}NNaO_4S$, 290.0458, found 290.0458.

Mass Spectrometry

Prior to mass spectrometric analysis hCA II protein was concentrated and buffer exchanged into 10 mM NH_4OAc pH 7.0 using Amicon Ultra 0.5 centrifugal filters (Merck Millipore, Sydney, NSW, Australia). In detail, 500 µL of the initial protein solution was loaded on the filter and centrifuged at 14,000 × g for 15 min at 4 °C on a Heraeus Pico 21 benchtop centrifuge (Thermo Fisher Scientific Australia Pty Ltd). The flow through was discarded and the concentrate resuspended in 450 µL of 10 mM NH_4OAc pH 7.0. This process was repeated four times in order to minimise residual salt in the protein sample that may interfere with protein ionisation. The final concentrate was recovered by spinning at 3,000 × g for 1 min according to the manufacturers protocol. Concentration of the proteins was verified for CA II using the absorption at 280 nm combined with an extinction coefficient of 50.42 x 10^3 M^{-1} cm^{-1} and

adjusted to a final concentration of 15 μM with 10 mM NH_4OAc, pH 7.0. All test fragments were prepared and stored as 5 mM stock solutions in DMSO.

For experiments with equimolar concentration of protein and fragment, immediately before the mass spectrometric analysis, fragments were diluted in 10 mM NH_4OAc 7.0 pH to a final concentration of 15 μM (0.3% DMSO). hCA II (2.5 μL of 15 μM stock) was mixed with fragment solution (2.5 μL of 15 μM stock). For nanoESI-MS titration experiments, 0.5 μL of the required fragment concentration in DMSO were prepared in assay-ready 96-well microplates by Compounds Australia (www.compoundsaustralia.com). Prior to analysis 14.5 μL of protein (15 μM, 10 mM NH_4OAc) was added to each fragment containing microplate well (final sample 3.3% DMSO). The protein:fragment sample solutions were mixed, then incubated for 10 min at room temperature before nanoESI-MS analysis. The incubation time was selected following time series test experiments which showed that no change in binding is observed after 10 min. FTICR-MS calibration using perfluorohexanoic acid (PFHA) was performed daily while quality control runs of pure CA II were performed before every batch of screening. For nanoESI-MS analysis samples were infused into a Bruker solariX XR™ 12.0 Tesla Fourier Transform Ion Cyclotron Resonance (FT-ICR) mass spectrometer (FT-ICR MS) fitted with a ParaCell™ (Bruker Daltonics Inc., Billerica, MA) using a Triversa Nanomate (Advion BioSciences, Ithaca, NY, USA) automated nanoESI interface fitted with a 5 micron HD A ESI Chip (Advion BioSciences, Ithaca, NY, USA). Spray conditions were optimized for signal intensity, signal to noise ratio and spray duration. Positive ion ESI was used with a capillary voltage of 1.2 kV and a nitrogen nebulizing gas pressure of 0.4 psi. The FT-ICR mass spectrometer parameters were optimised to maximise signal intensity whilst ensuring gentle enough conditions in order to retain the proteins in a native-like state and avoid in-source

dissociation. In detail, data were acquired for at least 45 scans, over the range of *m/z* 500-10,000 with the quadrupole set at *m/z* 600 while a Skimmer 1 voltage of 30 V, a Drying Gas Temperature of 100 ^{o}C, a Nebulizer Gas Flow Rate of 2 bar, a Capillary Voltage of 3,500 V, a Spray Shield of 500 V, a Collision Voltage (Entrance) of -3.0 V, a DC Extract Bias of 0.1 V, a Collision Cell RF of 2,000 Vpp, an Ion Accumulation Time of 0.001 sec and a Flight Time of 2.1 msec were used. Mass spectra were processed with Bruker Compass DataAnalysis 4.2 (Bruker Daltonics Inc., Billerica, MA). For the peak determination and intensity calculation, SNAP algorithm version 2.0 was used with a signal to noise threshold set at 3 and quality factor threshold set at 0.5.

The FA_{MS} for each fragment concentration was assigned as the ratio of the measured intensity of the fragment-bound protein $I_{(P:F)}$ peak to the sum of the unbound protein $I_{(P)}$ and fragment-bound protein $I_{(P:F)}$ peaks for each spectrum, expressed as a percentage (Equation 1). Unbound protein $I_{(P)}$ included both free protein and protein bound to acetate, the latter complex is preserved due to the very gentle electrospray ionisation conditions employed.

$$FA_{MS} = \frac{I_{[P:F]}}{I_{[P:F]}+I_{[P]}} \times 100\% \qquad \text{(Equation 1)}$$

All three observed charge states (+9, +10 and +11) where utilised for the FA_{MS} calculations and compared to FA_{MS} calculations using the predominant charge state (+10). For the analyses of the saturation binding experiments we employed the nonlinear Hill model.[73] The calculation of K_D value as well as curve fitting were performed by applying the Specific binding with Hill Slope equation in GraphPad Prism 7.01 (Equation 2), also using all three observed charge states (+9, +10 and +11) and the single, predominant charge state (+10) for comparison.

$$\frac{\text{Bound}}{\text{TotalProtein}} = \text{Bmax} * \frac{\text{FragmentConcentration}^{h}}{\text{Kd}^{h}+\text{FragmentConcentration}^{h}} \quad \text{(Equation 2)}$$

In equation 2 *Bmax* corresponds to the maximum specific binding, *Kd* to the fragment concentration needed to achieve a half-maximum binding at equilibrium and *h* to the Hill slope, which equals 1.0 when a monomer fragment binds to a single site of the protein.

SPR

Fragments were screened against biotinylated CA II with SPR as previously described.note The CA II protein was expressed and purified as previously described.[22] In brief, SPR dose-response experiments were performed at 25 °C. Fresh 100 mM DMSO fragment solutions were diluted directly with the fragment binding buffer to a final concentration of 200 μM and then diluted to 12.5 μM aiming for a 5-point concentration series range for the SPR dose-response experiment. Each compound was injected for 30 s association and 60 s dissociation. Scrubber 2 (www.biologic.com.au) and Microsoft Excel software packages were utilised for data processing and analysis.[74] To determine K_D values from dose-response experiments, binding responses at equilibrium were fit to a 1:1 steady state affinity model available within Scrubber.

Protein X-ray Crystallography.

Concentrated CA II at ~10 mg mL^{-1} was set up in SD-2 plates (Molecular Dimensions) with the following ratio of protein plus reservoir plus seeds: 250 nL + 225 nL + 25 nL. The plate was incubated at 8 ºC and the reservoir condition consisted of 2.9 M $(NH_4)_2SO_4$ sulfate with 0.1 M Tris buffer at pH 8.3. Dry compound was added to the crystallisation drop after crystals had formed and several days before data were collected. 360 frames of one degree oscillation were taken at the MX-1 beamline of the Australian Synchrotron. The data were indexed using

XDS[75] and scaled using Aimless.[76] Molecular replacement was done using Phaser[77] using 4cq0 as the initial starting model. The model was manually rebuilt using Coot[78] and refined using Refmac.[79] The compound was placed in density using the program Afitt (OpenEye Scientific Software) and further refined using Refmac.[79] The structure and structure factors were deposited in the PDB with accession codes: 5TXY, 5TY8, 5TY9, 5TYA, 5U0D, 5U0E, 5U0F, 5U0G and 5VGY.

Crystals with compound **10** (PDB code 5TXY) were generated by co-crystallisation. For these crystals, a six molar excess of compound to protein was added prior to the protein being set up in crystallisation trials. The data were processed as above, but Phenix[80] was used to refine the structure. eLBOW[81] was used to generate the cif dictionary file and the ligand was manually placed into density.

Corresponding author

S.-A.P. Telephone: +61 7 3735 7825; e-mail: s.poulsen@griffith.edu.au

T.S.P. Telephone: +61 3 9662 7304; e-mail: tom.peat@csiro.au

Acknowledgement

This research was financed by the Australian Research Council (Grant numbers DP140101495, FT10100185). We thank Griffith University for PhD Scholarship to P.M. cDNA for CA II was kindly provided by C. Fierke. We thank OpenEye Scientific Software for a license to use Afitt, the CSIRO Collaborative Crystallisation Centre (www.csiro.au/c3) for crystallisation, and the Australian Synchrotron and the beamline scientists at the MX-1 beamline for their support in data collection. We thank J. Bentley for help with protein purification, M. Hattarki for SPR

technical assistance, J. Ryan and T. Nebl for chemistry and mass spectrometry advice. We thank Compounds Australia staff for assistance in the production of assay-ready microplates (www.compoundsaustralia.com).

Abbreviations Used

FBDD, fragment based drug discovery; CA, carbonic anhydrase; CSIRO, Commonwealth Scientific and Industrial Research Organisation; HTS, high throughput screening; K_D, dissociation constant; SPR, surface plasmon resonance; MS, mass spectrometry; FA_{MS}, Fragment Affinity by mass spectrometry; FDA, food and drug administration; HEPES, 4-(2-hydroxyethyl)-1-piperazineethanesulfonic acid; PBS, phosphate buffered saline; XRC, X-ray crystallography

Supporting Information. Data collection and structure refinement statistics of fragment:hCA II crystal structures, NMR spectra and SPR sensorgrams for compounds. This material is available free of charge via the Internet at http://pubs.acs.org.

PDB ID Codes. All of the coordinates and structure factors have been deposited in the PDB and are available with the following codes: 5TXY, 5TY8, 5TY9, 5TYA, 5U0D, 5U0E, 5U0F, 5U0G, 5VGY.

References

Table of Contents Graphic

1. Rouffet, M.; Cohen, S. M. Emerging trends in metalloprotein inhibition. *Dalton Trans* **2011**, *40*, 3445-54.
2. Anzellotti, A. I.; Farrell, N. P. Zinc metalloproteins as medicinal targets. *Chem Soc Rev* **2008**, *37*, 1629-51.
3. Supuran, C. T. Carbonic anhydrase inhibitors in the treatment and prophylaxis of obesity. *Expert Opin. Ther. Patents* **2003**, *13*, 1545-1550.
4. Bull, S.; Loudon, M.; Francis, J. M.; Joseph, J.; Gerry, S.; Karamitsos, T. D.; Prendergast, B. D.; Banning, A. P.; Neubauer, S.; Myerson, S. G. A prospective, double-blind, randomized controlled trial of the angiotensin-converting enzyme inhibitor Ramipril In Aortic Stenosis (RIAS trial). *Eur Heart J Cardiovasc Imaging* **2015**, *16*, 834-41.
5. Paris, M.; Porcelloni, M.; Binaschi, M.; Fattori, D. Histone deacetylase inhibitors: from bench to clinic. *J Med Chem* **2008**, *51*, 1505-29.
6. Fernandez-Montero, J. V.; Vispo, E.; Soriano, V. Emerging antiretroviral drugs. *Expert Opin Pharmacother* **2014**, *15*, 211-9.
7. Zastrow, M. L.; Pecoraro, V. L. Designing Hydrolytic Zinc Metalloenzymes. *Biochemistry* **2014**, *53*, 957-978.
8. Andreini, C.; Banci, L.; Bertini, I.; Rosato, A. Counting the zinc-proteins encoded in the human genome. *J Proteome Res* **2006**, *5*, 196-201.
9. Martin, D. P.; Blachly, P. G.; McCammon, J. A.; Cohen, S. M. Exploring the influence of the protein environment on metal-binding pharmacophores. *J Med Chem* **2014**, *57*, 7126-35.
10. Zhang, X. X.; Liao, C. Perspectives in Medicinal Chemistry: Metalloprotein Inhibitors: What Have We Made and What is the Next Step? *Curr Top Med Chem* **2016**, *16*, 467-9.
11. Yang, Y.; Hu, X. Q.; Li, Q. S.; Zhang, X. X.; Ruan, B. F.; Xu, J.; Liao, C. Metalloprotein Inhibitors for the Treatment of Human Diseases. *Curr Top Med Chem* **2016**, *16*, 384-96.
12. Jacobsen, J.; Fullagar, J.; Miller, M.; Cohen, S. Identifying Chelators for Metalloprotein Inhibitors Using a Fragment-Based Approach. *J. Med. Chem.* **2011**, *54*, 591-602.
13. Dupont, C. L.; Yang, S.; Palenik, B.; Bourne, P. E. Modern proteomes contain putative imprints of ancient shifts in trace metal geochemistry. *Proc Natl Acad Sci U S A* **2006**, *103*, 17822-7.
14. Kawai, K.; Nagata, N. Metal-ligand interactions: an analysis of zinc binding groups using the Protein Data Bank. *Eur. J. Med. Chem.* **2012**, *51*, 271-276.
15. Scott, D. E.; Coyne, A. G.; Hudson, S. A.; Abell, C. Fragment-Based Approaches in Drug Discovery and Chemical Biology. *Biochemistry* **2012**, *51*, 4990−5003.
16. Erlanson, D. A.; Fesik, S. W.; Hubbard, R. E.; Jahnke, W.; Jhoti, H. Twenty years on: the impact of fragments on drug discovery. *Nat. Rev. Drug Discov.* **2016**, *15*, 605-619.
17. Agrawal, A.; Johnson, S. L.; Jacobsen, J. A.; Miller, M. T.; Chen, L.-H.; Pellecchia, M.; Cohen, S. M. Chelator fragment libraries for targeting metalloproteinases. *ChemMedChem* **2010**, *5*, 195–199.
18. Credille, C. V.; Chen, Y.; Cohen, S. M. Fragment-Based Identification of Influenza Endonuclease Inhibitors. *J. Med. Chem.* **2016**, *59*, 6444-6454.
19. Wischeler, J.; Innocenti, A.; Vullo, D.; Agrawal, A.; Cohen, S.; Heine, A.; Supuran, C.; Klebe, G. Bidentate Zinc Chelators for a-Carbonic Anhydrases that Produce a Trigonal Bipyramidal Coordination Geometry. *ChemMedChem* **2010**, *5*, 1609 – 1615.

20. Maresca, A.; Temperini, C.; Vu, H.; Pham, N. B.; Poulsen, S.-A.; Scozzafava, A.; Quinn, R. J.; Supuran, C. T. Non-zinc mediated inhibition of carbonic anhydrases: Coumarins are a new class of suicide inhibitors. *J. Am. Chem. Soc.* **2009**, *131*, 3057-3062.
21. Davis, R. A.; Vullo, D.; Maresca, A.; Supuran, C. T.; Poulsen, S.-A. Natural product coumarins that inhibit human carbonic anhydrases. *Bioorg. Med. Chem.* **2013**, *21*, 1539-1543.
22. Moeker, J.; Peat, T. S.; Bornaghi, L. F.; Vullo, D.; Supuran, C. T.; Poulsen, S.-A. Cyclic Secondary Sulfonamides: Unusually Good Inhibitors of Cancer-Related Carbonic Anhydrase Enzymes. *J. Med. Chem.* **2014**, *57*, 3522-3531.
23. Poulsen, S.-A. Direct screening of a dynamic combinatorial library using mass spectrometry. *J. Am. Soc. Mass Spectrom.* **2006**, *17*, 1074-1080.
24. Kopecka, J.; Rankin, G. M.; Salaroglio, I. C.; Poulsen, S. A.; Riganti, C. P-glycoprotein-mediated chemoresistance is reversed by carbonic anhydrase XII inhibitors. *Oncotarget* **2016**, *7*, 85861-85875.
25. Supuran, C. T. Carbonic anhydrases: novel therapeutic applications for inhibitors and activators. *Nat. Rev. Drug Discov.* **2008**, *7*, 168-181.
26. Parks, S. K.; Cormerais, Y.; Durivault, J.; Pouyssegur, J. Genetic disruption of the pHi-regulating proteins Na+/H+ exchanger 1 (SLC9A1) and carbonic anhydrase 9 severely reduces growth of colon cancer cells. *Oncotarget* **2016**, *in press*.
27. Poulsen, S. Carbonic anhydrase inhibition as a cancer therapy: a review of patent literature, 2007-2009. *Expert Opin. Ther. Patents* **2010**, *20*, 795-806.
28. Mujumdar, P.; Teruya, K.; Tonissen, K.; Vullo, D.; Supuran, C.; Peat, T.; Poulsen, S.-A. An Unusual Natural Product Primary Sulfonamide: Synthesis, Carbonic Anhydrase Inhibition, and Protein X-ray Structures of Psammaplin C. *J. Med. Chem.* **2016**, *59*.
29. Woods, L.; Dolezal, O.; Ren, B.; Ryan, J.; Peat, T.; Poulsen, S. Native State Mass Spectrometry, Surface Plasmon Resonance, and X-ray Crystallography Correlate Strongly as a Fragment Screening Combination. *J. Med. Chem.* **2016**, *59*, 2192–2204.
30. Ryde, U. Carboxylate binding modes in zinc proteins: a theoretical study. *Biophys J* **1999**, *77*, 2777-87.
31. Jacobsen, J. A.; Major Jourden, J. L.; Miller, M. T.; Cohen, S. M. To bind zinc or not to bind zinc: an examination of innovative approaches to improved metalloproteinase inhibition. *Biochim Biophys Acta* **2010**, *1803*, 72-94.
32. Liang, J.; Lipscomb, W. N. Binding of sulfonamide and acetamide to the active-site Zn2+ in carbonic anhydrase: a theoretical study. *Biochemistry* **1989**, *28*, 9724-33.
33. Boriack, P. A.; Christianson, D. W.; Kingery-Wood, J.; Whitesides, G. M. Secondary interactions significantly removed from the sulfonamide binding pocket of carbonic anhydrase II influence inhibitor binding constants. *J Med Chem* **1995**, *38*, 2286-91.
34. Martin, D.; Hann, Z.; Cohen, S. Metalloprotein–Inhibitor Binding: Human Carbonic Anhydrase II as a Model for Probing Metal–Ligand Interactions in a Metalloprotein Active Site. *Inorganic Chemistry* **2013**, *52*, 12207–12215.
35. Swayze, E. E.; Jefferson, E. A.; Sannes-Lowery, K. A.; Blyn, L. B.; Risen, L. M.; Arakawa, S.; Osgood, S. A.; Hofstadler, S. A.; Griffey, R. H. SAR by MS: a ligand based technique for drug lead discovery against structured RNA targets. *J. Med. Chem.* **2002**, *45*, 3816-9.
36. Alterio, V.; Di Fiore, A.; D'Ambrosio, K.; Supuran, C. T.; De Simone, G. Multiple binding modes of inhibitors to carbonic anhydrases: How to design specific drugs targeting 15 different isoforms? *Chem. Rev.* **2012**, *112*, 4421-4468.
37. Lipinski, C.; Fiese, E. F.; Korst, R. J. pKa, Log P and MedChem CLOGP fragment values of acidic heterocyclic potential bioisosteres. *Quant. Struct.-Act. Relat.* **1991**, *10*, 109-117.

38. Liu, W.; Lau, F.; Liu, K.; Wood, H. B.; Zhou, G.; Chen, Y.; Li, Y.; Akiyama, T. E.; Castriota, G.; Einstein, M.; Wang, C.; McCann, M. E.; Doebber, T. W.; Wu, M.; Chang, C. H.; McNamara, L.; McKeever, B.; Mosley, R. T.; Berger, J. P.; Meinke, P. T. Benzimidazolones: A New Class of Selective Peroxisome Proliferator Activated Receptor γ (PPARγ) Modulators. *J. Med. Chem.* **2011**, *54*, 8541−8554.
39. Hofstadler, S. A.; Sannes-Lowery, K. A. Applications of ESI-MS in drug discovery: interrogation of noncovalent complexes. *Nat. Rev. Drug Discov.* **2006**, *5*, 585-595.
40. Leney, A. C.; Heck, A. J. R. Native Mass Spectrometry: What is in the Name? *J. . Am. Soc. Mass Spectrom.* **2017**, *28*, 5-13.
41. Vivat-Hannah, V.; Atmanene, C.; Zeyer, D.; Van Dorsselaer, A.; Sanglier-Cianférani, S. Native MS: an 'ESI, way to support structure - and fragment-based drug discovery. *Future Med. Chem.* **2010**, *2*, 35-50.
42. Maple, H. J.; Garlish, R. A.; Rigau-Roca, L.; Porter, J.; Whitcombe, I.; Prosser, C. E.; Kennedy, J.; Henry, A. j.; Taylor, R. J.; Crump, M. P.; Crosby, J. Automated Protein−Ligand Interaction Screening by Mass Spectrometry. *J. Med. Chem.* **2012**, *55*, 837-851.
43. Drinkwater, N.; Vu, H.; Lovell, K. M.; Criscione, K. R.; Collins, B. M.; Prisinzano, T. E.; Poulsen, S.-A.; McLeish, M. J.; Grunewald, G. L.; Martin, J. L. Fragment-based screening by X-ray crystallography, MS and isothermal titration calorimetry to identify PNMT (phenylethanolamine N-methyltransferase) inhibitors *Biochem. J.* **2010**, *431*, 51-61.
44. Poulsen, S.-A. Fragment Screening by Native State Mass Spectrometry. *Aust. J. Chem.* **2013**, *66*, 1495–1501.
45. Pedro, L.; Quinn, R. J. Native Mass Spectrometry in Fragment-Based Drug Discovery. *Molecules* **2016**, *21*, 984.
46. Hulme, E. C.; Trevethick, M. A. Ligand binding assays at equilibrium: validation and interpretation. *Br J Pharmacol* **2010**, *161*, 1219-37.
47. Ermolenko, L.; Zhaoyu, H.; Lejeune, C.; Vergne, C.; Ratinaud, C.; Nguyen, T. B.; Al-Mourabit, A. Concise synthesis of Didebromohamacanthin A and Demethylaplysinopsine: Addition of Ethylenediamine and Guanidine Derivatives to the Pyrrole-Amino Acid Diketopiperazines in Oxidative Conditions. *Org. Lett.* **2014**, *16*, 872-875.
48. Baell, J. B.; Holloway, G. A. New Substructure Filters for Removal of Pan Assay Interference Compounds (PAINS) from Screening Libraries and for Their Exclusion in Bioassays. *J. Med. Chem.* **2010**, *53*, 2719-2740.
49. Oikonomakos, N. G., Skamnaki, V.T., Osz, E., Szilagyi, L., Somsak, L., Docsa, T., Toth, B., Gergely, P. Kinetic and crystallographic studies of glucopyranosylidene spirothiohydantoin binding to glycogen phosphorylase B. *bioorg Med Chem* **2002**, *10*, 261-268.
50. Zidar, N.; Tomasic, T.; Sink, R.; Rupnik, V.; Kovac, A.; Turk, S.; Patin, D.; Blanot, D.; Contreras Martel, C.; Dessen, A.; Muller Premru, M.; Zega, A.; Gobec, S.; Peterlin Masic, L.; Kikelj, D. Discovery of novel 5-benzylidenerhodanine and 5-benzylidenethiazolidine-2,4-dione inhibitors of MurD ligase. *J. Med. Chem.* **2010**, *53*, 6584-94.
51. Tomasic, T.; Zidar, N.; Sink, R.; Kovac, A.; Blanot, D.; Contreras-Martel, C.; Dessen, A.; Muller-Premru, M.; Zega, A.; Gobec, S.; Kikelj, D.; Masic, L. P. Structure-based design of a new series of D-glutamic acid based inhibitors of bacterial UDP-N-acetylmuramoyl-L-alanine:D-glutamate ligase (MurD). *J. Med. Chem.* **2011**, *54*, 4600-10.
52. Tomasic, T., Sink, R., Zidar, N., Fic, A., Contreras-Martel, C., Dessen, A., Patten, D., Blanot, D., Muller-Premru, M., Gobec, S., Zega, A., Kikelj, D., and Masic, L. P. . Dual Inhibitor of MurD and MurE Ligases from Escherichia coli and Staphylococcus aureus. *ACSMed.Chem.Lett.* **2012**, *3*, 626-630.
53. Nolte, R. T.; Wisely, G. B.; Westin, S.; Cobb, J. E.; Lambert, M. H.; Kurokawa, R.; Rosenfeld, M. G.; Willson, T. M.; Glass, C. K.; Milburn, M. V. Ligand binding and co-activator assembly of the peroxisome proliferator-activated receptor-gamma. *Nature* **1998**, *395*, 137-43.

54. Binda, C.; Aldeco, M.; Geldenhuys, W. J.; Tortorici, M.; Mattevi, A.; Edmondson, D. E. Molecular Insights into Human Monoamine Oxidase B Inhibition by the Glitazone Anti-Diabetes Drugs. *ACS Med Chem Lett* **2011**, *3*, 39-42.
55. Good, A. C.; Liu, J.; Hirth, B.; Asmussen, G.; Xiang, Y.; Biemann, H. P.; Bishop, K. A.; Fremgen, T.; Fitzgerald, M.; Gladysheva, T.; Jain, A.; Jancsics, K.; Metz, M.; Papoulis, A.; Skerlj, R.; Stepp, J. D.; Wei, R. R. Implications of promiscuous Pim-1 kinase fragment inhibitor hydrophobic interactions for fragment-based drug design. *J. Med. Chem.* **2012**, *55*, 2641-8.
56. Hughes, S. J.; Millan, D. S.; Kilty, I. C.; Lewthwaite, R. A.; Mathias, J. P.; O'Reilly, M. A.; Pannifer, A.; Phelan, A.; Stuhmeier, F.; Baldock, D. A.; Brown, D. G. Fragment based discovery of a novel and selective PI3 kinase inhibitor. *Bioorg. Med. Chem. Lett.* **2011**, *21*, 6586-90.
57. Dakin, L. A.; Block, M. H.; Chen, H.; Code, E.; Dowling, J. E.; Feng, X.; Ferguson, A. D.; Green, I.; Hird, A. W.; Howard, T.; Keeton, E. K.; Lamb, M. L.; Lyne, P. D.; Pollard, H.; Read, J.; Wu, A. J.; Zhang, T.; Zheng, X. Discovery of novel benzylidene-1,3-thiazolidine-2,4-diones as potent and selective inhibitors of the PIM-1, PIM-2, and PIM-3 protein kinases. *Bioorg. Med. Chem. Lett.* **2012**, *22*, 4599-604.
58. Camps, M.; Ruckle, T.; Ji, H.; Ardissone, V.; Rintelen, F.; Shaw, J.; Ferrandi, C.; Chabert, C.; Gillieron, C.; Francon, B.; Martin, T.; Gretener, D.; Perrin, D.; Leroy, D.; Vitte, P. A.; Hirsch, E.; Wymann, M. P.; Cirillo, R.; Schwarz, M. K.; Rommel, C. Blockade of PI3Kgamma suppresses joint inflammation and damage in mouse models of rheumatoid arthritis. *Nature medicine* **2005**, *11*, 936-43.
59. Richardson, C. M.; Nunns, C. L.; Williamson, D. S.; Parratt, M. J.; Dokurno, P.; Howes, R.; Borgognoni, J.; Drysdale, M. J.; Finch, H.; Hubbard, R. E.; Jackson, P. S.; Kierstan, P.; Lentzen, G.; Moore, J. D.; Murray, J. B.; Simmonite, H.; Surgenor, A. E.; Torrance, C. J. Discovery of a potent CDK2 inhibitor with a novel binding mode, using virtual screening and initial, structure-guided lead scoping. *Bioorg. Med. Chem. Lett.* **2007**, *17*, 3880-5.
60. Zidar, N.; Tomasic, T.; Sink, R.; Kovac, A.; Patin, D.; Blanot, D.; Contreras-Martel, C.; Dessen, A.; Premru, M. M.; Zega, A.; Gobec, S.; Masic, L. P.; Kikelj, D. New 5-benzylidenethiazolidin-4-one inhibitors of bacterial MurD ligase: design, synthesis, crystal structures, and biological evaluation. *Eur J Med Chem* **2011**, *46*, 5512-23.
61. Gillilan, R. E.; Ayers, S. D.; Noy, N. Structural basis for activation of fatty acid-binding protein 4. *J Mol Biol* **2007**, *372*, 1246-60.
62. Yu, W.; Guo, Z.; Orth, P.; Madison, V.; Chen, L.; Dai, C.; Feltz, R. J.; Girijavallabhan, V. M.; Kim, S. H.; Kozlowski, J. A.; Lavey, B. J.; Li, D.; Lundell, D.; Niu, X.; Piwinski, J. J.; Popovici-Muller, J.; Rizvi, R.; Rosner, K. E.; Shankar, B. B.; Shih, N.-Y.; Arshad Siddiqui, M.; Sun, J.; Tong, L.; Umland, S.; Wong, M. K. C.; Yang, D.-y.; Zhou, G. Discovery and SAR of hydantoin TACE inhibitors. *Bioorganic & medicinal chemistry letters* **2010**, *20*, 1877-1880.
63. Yu, W.; Tong, L.; Kim, S. H.; Wong, M. K.; Chen, L.; Yang, D. Y.; Shankar, B. B.; Lavey, B. J.; Zhou, G.; Kosinski, A.; Rizvi, R.; Li, D.; Feltz, R. J.; Piwinski, J. J.; Rosner, K. E.; Shih, N. Y.; Siddiqui, M. A.; Guo, Z.; Orth, P.; Shah, H.; Sun, J.; Umland, S.; Lundell, D. J.; Niu, X.; Kozlowski, J. A. Biaryl substituted hydantoin compounds as TACE inhibitors. *Bioorg. Med. Chem. Lett.* **2010**, *20*, 5286-9.
64. Durham, T. B.; Klimkowski, V. J.; Rito, C. J.; Marimuthu, J.; Toth, J. L.; Liu, C.; Durbin, J. D.; Stout, S. L.; Adams, L.; Swearingen, C.; Lin, C.; Chambers, M. G.; Thirunavukkarasu, K.; Wiley, M. R. Identification of potent and selective hydantoin inhibitors of aggrecanase-1 and aggrecanase-2 that are efficacious in both chemical and surgical models of osteoarthritis. *J. Med. Chem.* **2014**, *57*, 10476-85.
65. De Savi, C.; Waterson, D.; Pape, A.; Lamont, S.; Hadley, E.; Mills, M.; Page, K. M.; Bowyer, J.; Maciewicz, R. A. Hydantoin based inhibitors of MMP13--discovery of AZD6605. *Bioorg. Med. Chem. Lett.* **2013**, *23*, 4705-12.

66. Francesco, I. N.; Wagner, A.; Colobert, F. Suzuki–Miyaura Coupling Reaction of Boronic Acids and Ethyl Glyoxylate: Synthetic Access to Mandelate Derivatives. *Eur. J. Org. Chem.* **2008**, 5692-5695.
67. Sheehan, J. C.; Laubach, G. D. The Synthesis of Substituted Penicillins and Simpler Structural Analogs. V. The Application of 5-Phenyloxazolidine-2,4-diones to the Synthesis of Phenylacetylamino-β-lactams. *J. Am. Chem. Soc.* **1951**, *73*, 4752-4755.
68. Al-Horani, R. A.; Desai, U. R. Electronically rich N-substituted tetrahydroisoquinoline 3-carboxylic acid esters: concise synthesis and conformational studies. *Tetrahedron* **2012**, *68*, 2027-2040.
69. Tang, S. Q.; Lee, Y. Y. I.; Packiaraj, D. S.; Ho, H. K.; Chai, C. L. L. Systematic Evaluation of the Metabolism and Toxicity of Thiazolidinone and Imidazolidinone Heterocycles. *Chem. Res. Toxicol.* **2015**, *28*, 2019-2033.
70. Kottakota, S. K.; Benton, M.; Evangelopoulos, D.; Guzman, J. D.; Bhakta, S.; McHugh, T. D.; Gray, M.; Groundwater, P. W.; Marrs, E. C. L.; Perry, J. D.; Harburn, J. J. Versatile routes to marine sponge metabolites through benzylidene rhodanines. *Org. Lett.* **2012**, *14*, 6310-6313.
71. Giles, R. G.; Lewis, N. J.; Quick, J. K.; Sasse, M. J.; Urquhart, M. W. J.; Youssef, L. Regiospecific Reduction of 5-Benzylidene-2,4-Thiazolidinediones and 4-Oxo-2-thiazolidinethiones using Lithium Borohydride in Pyridine and Tetrahydrofuran. *Tetrahedron* **2000**, *56*, 4531-4537.
72. Willot, M.; Chen, J. C.; Zhu, J. Combination of Lithium Chloride and Hexafluoroisopropanol for Friedel-Crafts Reactions. *Syn. Lett.* **2009**, 577-580.
73. Goutelle, S.; Maurin, M.; Rougier, F.; Barbaut, X.; Bourguignon, L.; Ducher, M.; Maire, P. The Hill equation: a review of its capabilities in pharmacological modelling. *Fundam Clin Pharmacol* **2008**, *22*, 633-48.
74. Papalia, G. A.; Leavitt, S.; Bynum, M. A.; Katsamba, P. S.; Wilton, R.; Qiu, H.; Steukers, M.; Wang, S.; Bindu, L.; Phogat, S.; Giannetti, A. M.; Ryan, T. E.; Pudlak, V. A.; Matusiewicz, K.; Michelson, K. M.; Nowakowski, A.; Pham-Baginski, A.; Brooks, J.; Tieman, B. C.; Bruce, B. D.; Vaughn, M.; Baksh, M.; Cho, Y. H.; deWit, M.; Smets, A.; Vandersmissen, J.; Michiels, L.; Myszka, D. G. Comparative analysis of 10 small molecules binding to carbonic anhydrase II by different investigators using Biacore technology. *Anal. Biochem.* **2006**, *359*, 94−105.
75. Kabsch, W. XDS. *Acta Crystallogr. Sect. D: Biol. Crystallogr.* **2010**, *66*, 125-132.
76. Evans, P. R. An introduction to data reduction: space-group determination, scaling and intensity statistics. *Acta Crystallogr. D Biol. Crystallogr.* **2011**, *67*, 282-292.
77. McCoy, A. J.; Grosse-Kunstleve, R. W.; Adams, P. D.; Winn, M. D.; Storoni, L. C.; Read, R. J. Phaser crystallographic software. *J. Appl. Crystallogr.* **2007**, *40*, 658-674.
78. Emsley, P.; Lohkamp, B.; Scott, W. G.; Cowtan, K. Features and development of Coot. *Acta Crystallogr. D Biol. Crystallogr.* **2010**, *66*, 486-501.
79. Murshudov, G. N.; Skubak, P.; Lebedev, A. A.; Pannu, N. S.; Steiner, R. A.; Nicholls, R. A.; Winn, M. D.; Long, F.; Vagin, A. A. REFMAC5 for the refinement of macromolecular crystal structures. *Acta Crystallogr. D Biol. Crystallogr.* **2011**, *67*, 355-367.
80. Afonine, P. V.; Grosse-Kunstleve, R. W.; Echols, N.; Headd, J. J.; Moriarty, N. W.; Mustyakimov, M.; Terwilliger, T. C.; Urzhumtsev, A.; Zwart, P. H.; Adams, P. D. Towards automated crystallographic structure refinement with phenix.refine. *Acta Crystallogr. D Biol. Crystallogr.* **2012**, *68*, 352-367.
81. Moriarty, N. W.; Grosse-Kunstleve, R. W.; Adams, P. D. Electronic Ligand Builder and Optimization Workbench (eLBOW): a tool for ligand coordinate and restraint generation. *Acta Crystallogr. D* **2009**, *65*, 1074-1080.